JGR Atmospheres

RESEARCH ARTICLE
10.1029/2020JD034038

An Aerosol Climatology and Implications for Clouds at a Remote Marine Site: Case Study Over Bermuda

Abdulmonam M. Aldhaif[1], David H. Lopez[1], Hossein Dadashazar[1], David Painemal[2,3], Andrew J. Peters[4], and Armin Sorooshian[1,5]

[1]Department of Chemical and Environmental Engineering, University of Arizona, Tucson, AZ, USA, [2]Science Systems and Applications, Inc., Hampton, VA, USA, [3]NASA Langley Research Center, Hampton, VA, USA, [4]Bermuda Institute of Ocean Sciences, St. George's, Bermuda, [5]Department of Hydrology and Atmospheric Sciences, University of Arizona, Tucson, AZ, USA

Abstract Aerosol characteristics and aerosol–cloud interactions remain uncertain in remote marine regions. We use over a decade of data (2000–2012) from the NASA AErosol RObotic NETwork, aerosol and wet deposition samples, satellite remote sensors, and models to examine aerosol and cloud droplet number characteristics at a representative open ocean site (Bermuda) over the Western North Atlantic Ocean (WNAO). Annual mean values were as follows: aerosol optical depth (AOD) = 0.12, Ångström Exponent (440/870 nm) = 0.95, fine mode fraction = 0.51, asymmetry factor = 0.72 (440 nm) and 0.68 (1020 nm), and Aqua-MODIS cloud droplet number concentrations = 51.3 cm^{-3}. The winter season (December–February) was characterized by high sea salt optical thickness and the highest aerosol extinction in the lowest 2 km. Extensive precipitation over the WNAO in winter helps contribute to the low FMFs in winter (~0.40–0.50) even though air trajectories often originate over North America. Spring and summer had more pronounced influence from sulfate, dust, organic carbon, and black carbon. Volume size distributions were bimodal with a dominant coarse mode (effective radii: 1.85–2.09 μm) and less pronounced fine mode (0.14–0.16 μm), with variability in the coarse mode likely due to different characteristic sizes for transported dust (smaller) versus regional sea salt (larger). Extreme pollution events highlight the sensitivity of this site to long-range transport of urban emissions, dust, and smoke. Differing annual cycles are identified between AOD and cloud droplet number concentrations, motivating a deeper look into aerosol–cloud interactions at this site.

Key Points:

- While anthropogenic influence is lowest in winter, cloud drop number concentrations are close to peak values along with high sea salt levels
- Bimodal volume size distributions with a dominant coarse mode peak that shifts to smaller sizes in spring/summer due in part to dust
- Extreme pollution events show the sensitivity of remote marine sites like Bermuda to a continental outflow of urban emissions, dust, and smoke

Correspondence to:
A. Sorooshian,
armin@email.arizona.edu

Citation:
Aldhaif, A. M., Lopez, D. H., Dadashazar, H., Painemal, D., Peters, A. J., & Sorooshian, A. (2021). An aerosol climatology and implications for clouds at a remote marine site: Case study over Bermuda. *Journal of Geophysical Research: Atmospheres*, *126*, e2020JD034038. https://doi.org/10.1029/2020JD034038

Received 12 OCT 2020
Accepted 12 FEB 2021

Author Contributions:
Conceptualization: Abdulmonam M. Aldhaif, David H. Lopez
Formal analysis: Abdulmonam M. Aldhaif, David H. Lopez, Hossein Dadashazar
Funding acquisition: Armin Sorooshian
Investigation: Abdulmonam M. Aldhaif, Andrew J. Peters
Methodology: Abdulmonam M. Aldhaif, David H. Lopez, David Painemal
Project Administration: Armin Sorooshian
Supervision: Armin Sorooshian
Writing – original draft: Abdulmonam M. Aldhaif, Armin Sorooshian
Writing – review & editing: David H. Lopez, Hossein Dadashazar, David Painemal, Andrew J. Peters, Armin Sorooshian

1. Introduction

As oceans cover 71% of the global surface area, the characterization of marine regions in terms of their meteorological features and atmospheric chemistry is essential for a better understanding of air quality, climate, and the hydrological cycle. Remote marine areas influenced predominantly by natural aerosols are of particular interest as climate model uncertainties in aerosol radiative forcing depend on knowledge of pre-industrial aerosol conditions that were negligibly impacted by anthropogenic sources (Carslaw et al., 2010, 2017; Regayre et al., 2020). However, many islands in remote marine regions are not without anthropogenic influence (Smirnov et al., 2002), and such sites provide important natural laboratory settings to investigate aged plumes originating from sources such as fires, dust, and urban emissions. Although not pristine (Holben et al., 2001; Smirnov et al., 2002), the western North Atlantic Ocean (WNAO; defined here as 25–50°N and 60–85°W) has been extensively studied with the ship and airborne field campaigns as it represents an oceanic basin receiving aerosol and gas inputs from North Africa, East Asia, North, and Central America, Europe, and the ocean itself (Sorooshian et al., 2020). Field studies are short-lived owing to the logistical challenge of conducting them over long periods of time. The island of Bermuda therefore emerged as a critically important location for atmospheric research with the installation of a number of surface measurement sites. Datasets available for Bermuda afford the opportunity to characterize aerosols over a long-term period that is not possible with shorter intensive operational studies.

Approximately, 146 past studies were reviewed in a recent publication relevant to atmospheric research over Bermuda, with the majority of them devoted to aspects of atmospheric chemistry (Sorooshian et al., 2020). This island site is distinct from others such as in the Pacific Ocean basin owing to more pollution emanating from different seasonally dependent continental sources (Anderson et al., 1996; Arimoto et al., 2003;

Galloway et al., 1989; Holben et al., 2001; Moody et al., 1995; Smirnov et al., 2002; Wolff et al., 1986). This island is approximately 1050 km east of Cape Hatteras (North Carolina, USA), being ~2 km wide and ~30 km long. The population as of 2016 was ~64,000 (Government of Bermuda, 2019), with transported pollution significantly outweighing locally generated emissions in governing the atmospheric composition over the island (Galloway et al., 1988). Aside from gas and aerosol measurements, wet deposition samples demonstrate the influence of North American air masses in the form of elevated trace metals, SO_4^{2-}, and NO_3^- (Galloway et al., 1983; Jickells et al., 1982); that result not only highlights the sensitivity of this island to long-range transport but motivates research in Bermuda to gather insights into aerosol–cloud interactions as the chemical signature of continental plumes are evident in surface precipitation. Much can be learned about these interactions, which account for the largest uncertainty in global anthropogenic radiative forcing (IPCC, 2013), at a location such as Bermuda where there is a natural aerosol background but with the possibility of episodic perturbations associated with long-range transport.

One of the longest records of data from Bermuda capable of providing monthly statistics of aerosol properties is from the NASA AErosol RObotic NETwork (AERONET) (Holben et al., 1998). Previous research using AERONET data over Bermuda was limited to studying short time periods such as a few months (Aryal et al., 2014; Smirnov et al., 1998, 2000) and/or focused more on remote sensing retrieval and model assessment (Ahmad et al., 2010; Smirnov et al., 2003). The most relevant study to ours examined AERONET data at Bermuda between March 1996 and December 1999 (Smirnov et al., 2002). The goal of this work is to couple more recent and longer-term AERONET data from Bermuda to complementary datasets to address the following issues: (i) what are the characteristic monthly properties and relationships between aerosols, meteorology, and atmospheric flow patterns?; (ii) what are the regional monthly variations in cloud droplet number concentrations in relation to aerosol and wet deposition properties; and (iii) what are features of extreme pollution events in four different seasons at Bermuda? Results from this study are put into broader context via comparison to past studies involving similar types of data for Bermuda (Holben et al., 2001; Horvath et al., 1990; Kim et al., 1990; Korotaev et al., 1993; Smirnov et al., 2002). Findings from this work are not specific to just Bermuda but are broadly relevant to remote marine regions impacted by long-range transport of pollution, with implications for climate, air quality, cloud processes, and biogeochemical cycling of nutrients and contaminants.

2. Data and Methods

Table 1 provides an acronym summary and dataset details, which are briefly described below. Daily average values of data parameters are used for calculations.

2.1. Datasets

2.1.1. AERONET

One of the main motivations of using Bermuda as the anchor point of this analysis as a representative remote ocean site is that it offers long-term remote sensing data of aerosols from surface monitoring sites associated with AERONET (Holben et al., 1998; http://aeronet.gsfc.nasa.gov/). Level 2 daily data used here are cloud screened and quality assured (Eck et al., 1999; Holben et al., 2001) based on the Version 3 algorithm (Giles et al., 2019). Data are taken from the following three sites: Bermuda (32.37° N, 64.70° W) from February 2000 to December 2002, Prospect Hill (32.30° N, 64.77° W) from February 2005 to April 2006, and Tudor Hill (32.26° N, 64.88° W) from December 2007 to April 2012. Aerosol optical depth (AOD) values at 500 nm were converted to 550 nm by using a second-order polynomial fit of AOD retrieval data at different wavelengths (Eck et al., 1999). This conversion allows for a more direct comparison to MERRA-2 data at 550 nm. Uncertainties in AOD are reported to be <0.02 (Dubovik et al., 2000; Eck et al., 1999). Other relevant aerosol parameters used from AERONET include fine mode fraction (FMF), extinction Ångström exponent (AE) at 440/870 nm, asymmetry factor (ASY) at four wavelengths (440, 675, 870, 1020 nm), and volume size distributions (VSDs).

Table 1
Summary of Acronyms and Data Products Used in this Study, Including Data Parameter Name, Date Range of Data Collection, and Spatial Area Examined

Parameter	Acronym	Data source	Level	Resolution	Date range		Spatial area
Aerosol optical depth	AOD	AERONET	2	Hourly	03-Feb-2000	05-Apr-2012	See Section 2.1.1
Fine mode fraction	FMF	AERONET	2	Daily	03-Feb-2000	05-Apr-2012	See Section 2.1.1
Angstrom exponent (440–870 nm)	AE	AERONET	3	Daily	03-Feb-2000	05-Apr-2012	See Section 2.1.1
Asymmetry factor	ASY	AERONET	3	Daily	03-Feb-2000	05-Apr-2012	See Section 2.1.1
Volume size distribution	VSD	AERONET	3	Daily	03-Feb-2000	05-Apr-2012	See Section 2.1.1
Surface aerosol composition		Fort Prospect Station			01-Sep-1989	31-May-2011	64.77°W; 32.30°N
Surface wet deposition composition		Fort Prospect Station			01-Jul-1989	31-Oct-2012	64.77°W; 32.30°N
Cloud drop number concentration	N_d	CERES-MODIS	2	Daily	01-Jan-2013	31-Dec-2017	64°–65°W; 32°–33°N
Total and speciated aerosol optical thickness	AOT	MERRA-2	4	Hourly	01-Jan-2000	31-Dec-2012	64.375°–65°W; 32°–32.5°N
Dust AOT		MERRA-2	4	Hourly	01-Jan-2000	31-Dec-2012	64.375°–65°W; 32°–32.5°N
Sea salt AOT		MERRA-2	4	Hourly	01-Jan-2000	31-Dec-2012	64.375°–65°W; 32°–32.5°N
Black carbon AOT		MERRA-2	4	Hourly	01-Jan-2000	31-Dec-2012	64.375°–65°W; 32°–32.5°N
Sulfate AOT		MERRA-2	5	Hourly	01-Jan-2000	31-Dec-2012	64.375°–65°W; 32°–32.5°N
Organic carbon AOT		MERRA-2	4	Hourly	01-Jan-2000	31-Dec-2012	64.375°–65°W; 32°–32.5°N
Temperature (10 m)	T	MERRA	4	Daily	01-Jan-2000	31-Dec-2012	64°–66°W; 32°–32.5°N
Relative humidity	RH	MERRA	4	Daily	01-Jan-2000	31-Dec-2012	64.375°–65.625°W; 31.875°–33.125°N
Planetary boundary layer height	PBLH	MERRA	4	Daily	01-Jan-2000	31-Dec-2012	64°–66°W; 32°–32.5°N
Vertical aerosol extinction		CALIPSO		Daily	14-Jun-2006	31-Dec-2012	62.790°–66.790°W; 30.299°–34.299°N
Precipitation		PERSIANN		Daily	01-Mar-2000	31-Dec-2012	64.5°–65°W; 32.25°–32.75°N
Back-trajectory		HYSPLIT		N/A	01-Jan-2000	31-Dec-2012	64.66°W; 32.36°N
Additional acronyms							
Western North Atlantic Ocean	WNAO						
December–January–February	DJF						
March–April–May	MAM						
June–July–August	JJA						
September–October–November	SON						
Ratio of average radius weighted by geometrical cross-sectional area	R_{eff}						
Mean logarithm of the radius	R						
Geometric standard deviation	σ						
Cloud condensation nuclei	CCN						
Sea salt	SS						
Black carbon	BC						
Organic carbon	OC						

2.1.2. Surface Aerosol and Wet Deposition Samples

Co-located aerosol and wet deposition sampling was conducted at an ambient air quality monitoring station located at Fort Prospect in the center of Bermuda (32.30° N, 64.77°W) on the second-highest point on the island (63 m ASL) (https://doi.org/10.6084/m9.figshare.13651454.v1). As shown in Table 1, sampling was conducted between 1989 and either 2011 (aerosol) or 2012 (wet deposition); the use of data across a wider range than the other datasets is not considered an issue as the analysis focuses on monthly and seasonal trends that are not expected to change using a wider time range. Total suspended particle samples were collected on 47 mm diameter PTFE filters (Zefluor, pore size 1.0 μm, Pall Scientific) using a custom-built sampling system. The sampling flow rate was ~15 L min^{-1}. Aerosol samples were exchanged at the same time (+/− 1 h) on a daily basis, Monday through Friday, with composite samples being collected over weekends (i.e., Friday a.m. to Monday a.m.). Thus, all aerosol samples are of 24 or 72 h duration. Following sampling, the PTFE filters were sealed in clean polypropylene test tubes and frozen at −4 °C until analysis. After thawing, the filters were wetted with 140 μL methanol (residue grade, Burdick & Jackson) and extracted with 12 mL ultra-high purity water (Milli-Q) by sonication for 1 h, followed by storage overnight at 4 °C. Rainwater was collected following any events that provided sufficient volume for analysis, using automatic wet-dry precipitation samplers (Aerochem Metrics model 301 or Loda Electronics NADP samplers). Rainfall amount and volume of sampled water were recorded and aliquots were taken for immediate determination of specific conductivity and pH. Sub-samples for major ion analysis were stored in unused and cleaned 250 mL HDPE plastic bottles, preserved with 0.5 mL of chloroform, and stored at 4 °C.

Prior to 2010, anions were analyzed using a Dionex DX 100 model ion chromatograph and metallic cations were analyzed using a Perkin-Elmer AAnalyst 800 model spectrophotometer. After 2010, major ions in aerosol extracts and rainwater were determined in parallel using dual ion chromatography (IC). Anions were analyzed using a Dionex ICS-1600 IC equipped with an IonPac AS14A-5μm analytical column and AG14 A guard column, with 8 mM sodium carbonate and 1 mM sodium bicarbonate eluent. Cations were analyzed using a Dionex ICS-1500 IC equipped with an IonPac CS16 analytical column and CG16 guard column, with 47 mM methanesulfonic acid eluent. A comprehensive suite of replicate analyses, methods, and sample blanks were employed, and certified reference materials AES-05 Acid Rain Water and TROIS-94 River Water (Environment Canada) were used for QA/QC purposes. The focus of the aerosol and wet deposition data is sea salt tracer species (Cl^- and Na^+) and non-sea salt (nss) SO_4^{2-}.

2.1.3. CERES-MODIS

Daily cloud drop number concentrations (N_d) were estimated (Grosvenor et al., 2018) using Aqua MODerate resolution Imaging Spectroradiometer (MODIS)-based cloud effective radius, cloud optical depth, and temperature from Level 3 data (1 ° × 1 ° grid resolution) using an adiabatic framework documented in Painemal (2018). We used the Single Scanning Footprint daily product of the Cloud and the Earth's Radiant Energy System Edition 4 (CERES-MODIS; https://ceres.larc.nasa.gov/data/) (Minnis et al., 2011, 2020) obtained between 2013 and 2017 for the region encompassed by 31–34°N and 63–66°W surrounding Bermuda; although these data represent a different time period than other data used, the annual cycle is expected to be unaffected, which is our primary focus. We remove grids with cloud fraction <30% to minimize remote sensing artifacts in highly heterogeneous clouds scenes and more likely to be affected by clear-sky contamination (Painemal et al., 2013); cloud fraction values were obtained from the same CERES-MODIS Level 3 dataset for low-level liquid clouds with cloud top pressure >700 hPa.

2.1.4. MERRA and MERRA-2

Data from the Modern Era-Retrospective Analysis for Research and Applications (MERRA-2; https://disc.gsfc.nasa.gov/) are used for total and speciated aerosol optical thickness (AOT) at 550 nm (Bosilovich et al., 2015; Gelaro et al., 2017; Randles et al., 2017). Aerosol reanalysis products used from MERRA-2 are described elsewhere (Buchard et al., 2017; Randles et al., 2017). The speciated AOTs are for dust, sea salt, sulfate, organic carbon, and black carbon. Data for meteorological parameters (temperature, relative humidity, planetary boundary later height) are additionally used from MERRA (Rienecker et al., 2011).

2.1.5. CALIPSO

Vertical aerosol extinction profiles (532 nm) were obtained from the Cloud-Aerosol Lidar with Orthogonal Polarization (CALIOP) sensor onboard the Cloud-Aerosol Lidar and Infrared Pathfinder Satellite Observations (CALIPSO) satellite (Vaughan et al., 2009; Winker et al., 2009). We use day and nighttime 5 km aerosol profile data (version 4.20; Level 2) between 14 June 2006 and 2031 December 2012 (https://subset.larc.nasa.gov/calipso/). CALIPSO made a total of 410 daytime and 403 nighttime overpasses during that time frame in a 4 ° × 4 ° domain (62.790°–66.790°W and 30.299°–34.299°N) with Bermuda situated near the middle. We followed the guidance of Tackett et al. (2018) to apply quality control to Level 2 data with the following differences: (i) no aerosol layers were rejected based on data at 80 km resolution; and (ii) we did not exclude any detected clear-air samples with an aerosol layer base <250 m.

2.1.6. Precipitation

Surface precipitation data were obtained from the Precipitation Estimation from the Remotely Sensed Information using Artificial Neural Networks (PERSIANN: https://chrsdata.eng.uci.edu/) product (Nguyen et al., 2019). PERSIANN is a satellite-based precipitation retrieval algorithm that uses an artificial neural network model to convert infrared brightness imagery into rain rates (Hsu et al., 1997).

2.1.7. Air Mass Trajectory and Chemical Transport Modeling

The NOAA Hybrid Single-Particle Lagrangian Integrated Trajectory (HYSPLIT) model provided air mass back-trajectories (Rolph et al., 2017; Stein et al., 2015). National Centers for Environmental Prediction/National Center for Atmospheric Research (NCEP/NCAR) reanalysis data were used in conjunction with the "Model vertical velocity" method to generate 96 h back-trajectories starting every 6 h with an ending altitude of 0.5 km above Bermuda's ground level. This ending altitude has been used in similar types of studies examining aerosol characteristics for other regions (Crosbie et al., 2014; Mora et al., 2017; Sorooshian et al., 2011). Monthly back-trajectory density plots were generated for the period between January 2000 and December 2012 using TrajStat (Wang et al., 2009).

For extreme event analysis (Section 2.2), it was important to use chemical transport modeling to identify the predominant aerosol types(s) impacting Bermuda. For this purpose, we use both MERRA-2 and the Navy Aerosol Analysis and Prediction System (NAAPS) (Lynch et al., 2016; https://www.nrlmry.navy.mil/aerosol/), the latter of which relies on meteorological information from the Navy Global Environmental Model (NAVGEM) (Hogan et al., 2014). NAAPS is helpful for the identification of air mass types such as dust and smoke (e.g., Braun et al., 2020; Mardi et al., 2018; Maudlin et al., 2015; Schlosser et al., 2017; Wells et al., 2007; Xian et al., 2013).

2.2. Extreme Event Analysis

We examine the nature of anomalously high AOD days (i.e., extreme events). These days were identified based on daily AOD values from AERONET exceeding the average plus two times the standard deviation of AOD for that particular month when using all years of available data. AERONET was used in favor of other products such as MERRA-2 or MODIS as it is considered here to be the most reliable data product for AOD above Bermuda. The same type of criteria has been utilized in previous studies over the southwest U.S. (Lopez et al., 2016) and Mediterranean regions (Gkikas et al., 2009). These criteria resulted in days selected with AOD values exceeding the 94th percentile of AOD for each month. While we identified 71 extreme events, we select one representative case study for each of the four seasons. Both HYSPLIT and NAAPS were used as independent datasets to confirm the same air mass source region for each extreme event, with the latter used along with MERRA-2 to determine the predominant aerosol types.

3. Results and Discussion

3.1. Meteorology and Atmospheric Circulation

The transport patterns (Figure 1) and meteorological context (Figure 2) of Bermuda are discussed first. Previous work has already summarized environmental and flow conditions impacting Bermuda (Sorooshian et al., 2020 and references therein). One of the main climatological features over the WNAO region is

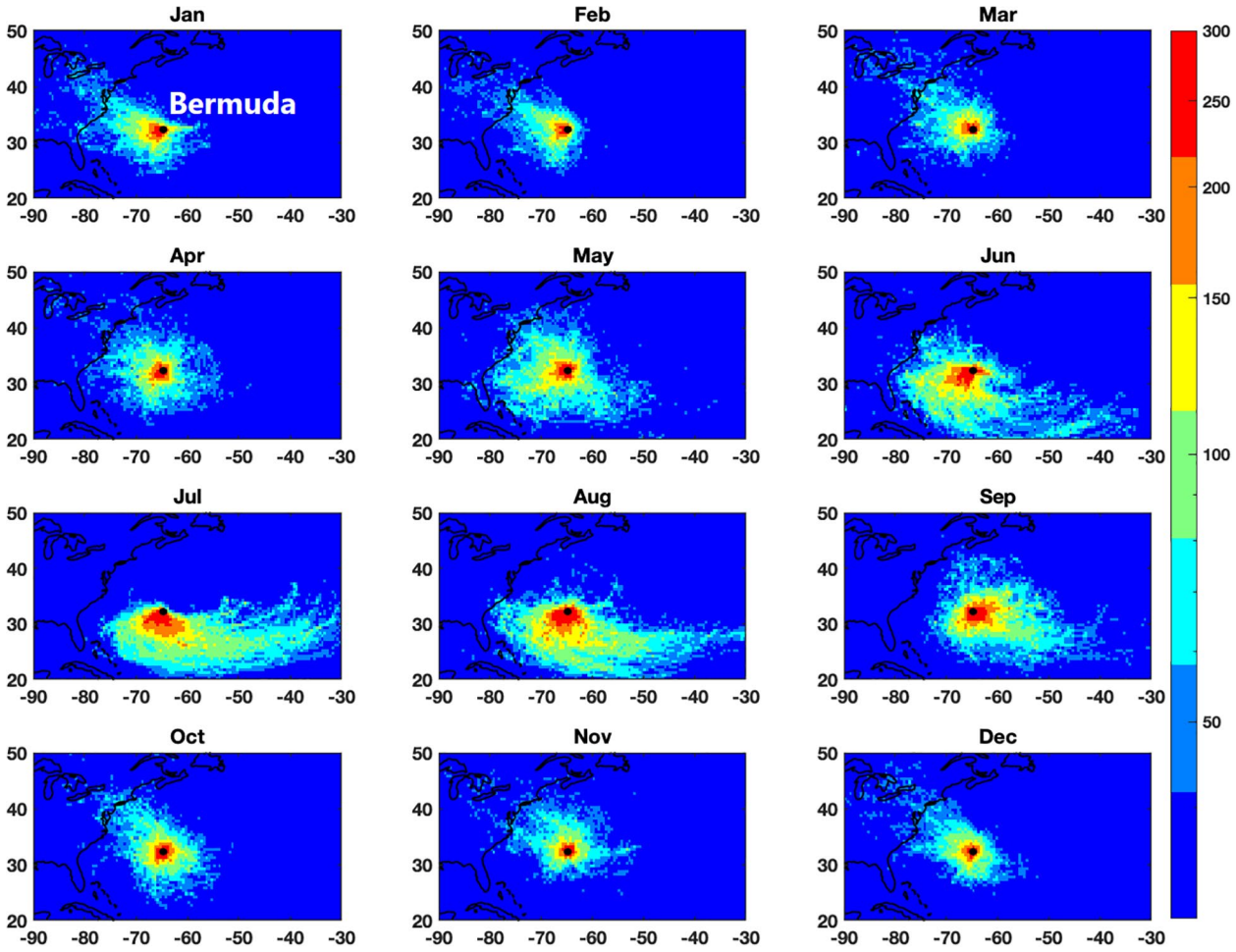

Figure 1. HYSPLIT back-trajectory density plots for each month, based on 240 h trajectories simulated every six h using the HYSPLIT reanalysis model ("global, 1948 to present") for the period between January 2000 and December 2012. The color bar is in logarithmic format and represents the number of back-trajectories passing through a particular pixel; while the color bar maximum value is set to 300 to view spatial variations better, the actual maximum value ranged from 2301 (February) to 4381 (August). Bermuda is denoted with a black marker and radiolabeled in the January panel.

the anticyclone, or Bermuda High, that develops most strongly in the summer with a flow pattern leading to easterly winds south of ~25°N that eventually turn north and flow southwesterly along the U.S. East Coast north of 25°N. Flow is centered around this subtropical anticyclone between May and November near Bermuda, with the other months being characterized more by westerly/northwesterly flow patterns (Merrill, 1994). Miller and Harris (1985) used multiple years of air back-trajectory data to show that North American outflow directly impacted Bermuda 60% of the time and that high precipitation periods were coincident with southeasterly and southwesterly winds. Past work suggested that the three characteristic sources impacting Bermuda were Saharan dust, North American air, and pure Atlantic air (Reddy et al., 1990; Smirnov et al., 2000). Our HYSPLIT data analysis reveals features consistent with the aforementioned studies based on monthly trajectory density plots (Figure 1). The period between October and May exhibits the highest density of trajectories coming from North America. In contrast, June through September showed more air transported from the southwest and southeast of Bermuda.

Figure 2a shows that near-surface temperature is lowest between December and April ranging from monthly median values of 17.8 °C–19.9 °C, with the minimum value in February. The highest monthly median temperatures were between July and September (26.6 °C–27.2 °C), peaking in August. Relative humidity (RH) generally followed a similar monthly trend as temperature, with the lowest median values in the colder months between October and April (72.6%–76.8%), with the minimum monthly value in December (Figure 2b). The highest median RH values were between June and August (82.2%–84.1%). Monthly

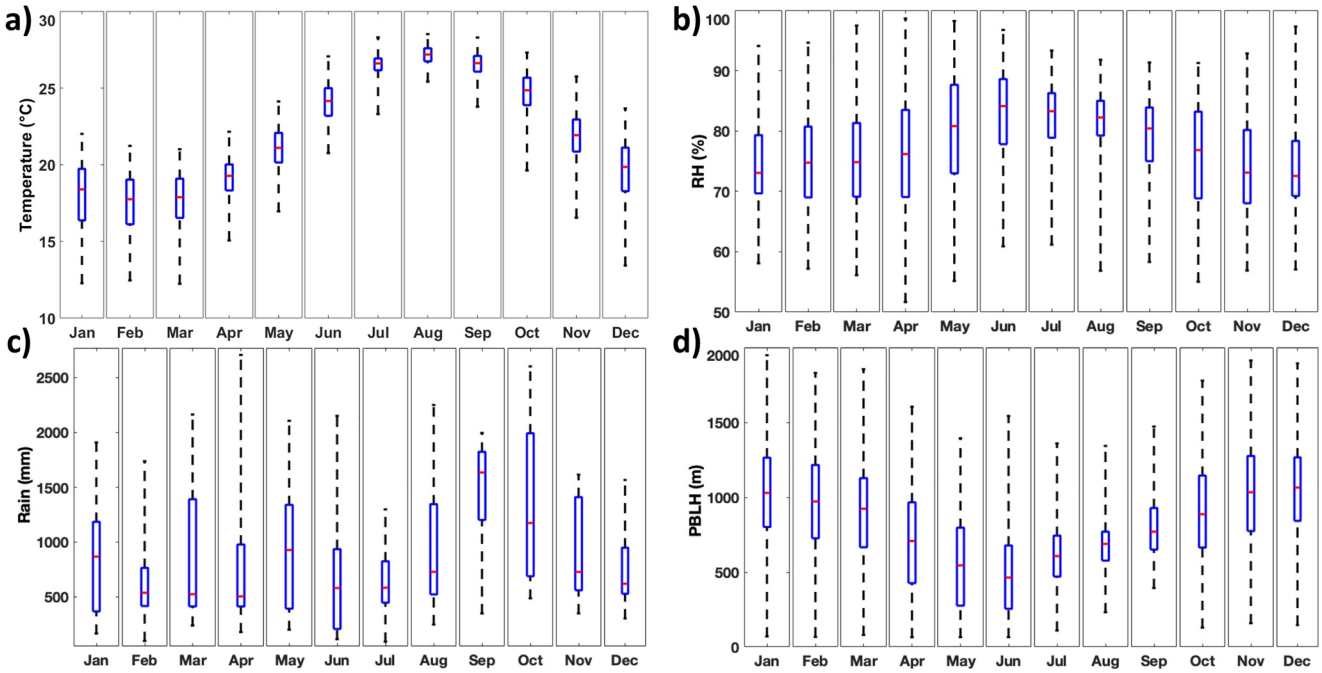

Figure 2. Monthly statistics for (a) MERRA temperature at 10 m above the displacement height, (b) MERRA relative humidity (RH) at 1000 hPa, (c) PERSIANN rain accumulation, and (d) MERRA planetary boundary layer height. Whiskers are the monthly range, red lines represent the median, and the top and bottom of the box represent the 75th and 25th percentile, respectively.

median rain accumulation varied from 505 mm in April to 1635 mm in September (Figure 2c). Galloway et al. (1993) reported that frontal and convective rains are responsible for the majority of precipitation in Bermuda, which is the case for the entire WNAO region (Sorooshian et al., 2020). Subtropical storms most frequently impact Bermuda in September and October (Guishard et al., 2007), which is evident in Figure 2c. Planetary boundary layer height (PBLH) exhibited its highest and lowest median values between November and January (1030–1065 m) and May and July (464–607 m), respectively (Figure 2d). It is not expected that PBLH will have a significant influence on the remotely sensed aerosol data, which are based on columnar values rather than boundary layer measurements that are more sensitive to PBLH (e.g., Dadashazar et al., 2019; Hersey et al., 2015; Hilario et al., 2020).

3.2. Aerosol Characteristics

3.2.1. Aerosol Optical Depth

There was a pronounced annual cycle in AERONET AOD with the highest monthly median values between March and August (0.10–0.14) with a peak in May (Figure 3a). In contrast, AOD exhibited its lowest median value (0.07) in November and January. The highest monthly standard deviations were observed between May and August (0.09–0.11). As will be shown, these months are most sensitive to episodic pollution events such as from dust and smoke. Many studies have shown that African dust reaches not just Bermuda but the southeast U.S. and areas like Barbados most frequently in the summer (Aldhaif et al., 2020; Arimoto, 2001; Muhs et al., 2012; Prospero, 1999; Prospero & Landing, 2009; Zuidema et al., 2019). Evidence of biomass burning reaching Bermuda in the summer was provided by Mead et al. (2013). The period between March and August exhibits the following features that can contribute to heightened AOD based on Figures 1 and 2: (i) highest monthly mean RH values leading to aerosol swelling via aerosol hygroscopic growth; (ii) lack of temporal overlap with the rainiest months, which would serve to reduce aerosol concentrations via wet scavenging; (iii) enhanced temperatures promoting secondary aerosol formation via gas-to-particle conversion processes; and (iv) long-range transport from both North America and to the southwest/southeast where a dust transport corridor resides stemming mainly from North Africa.

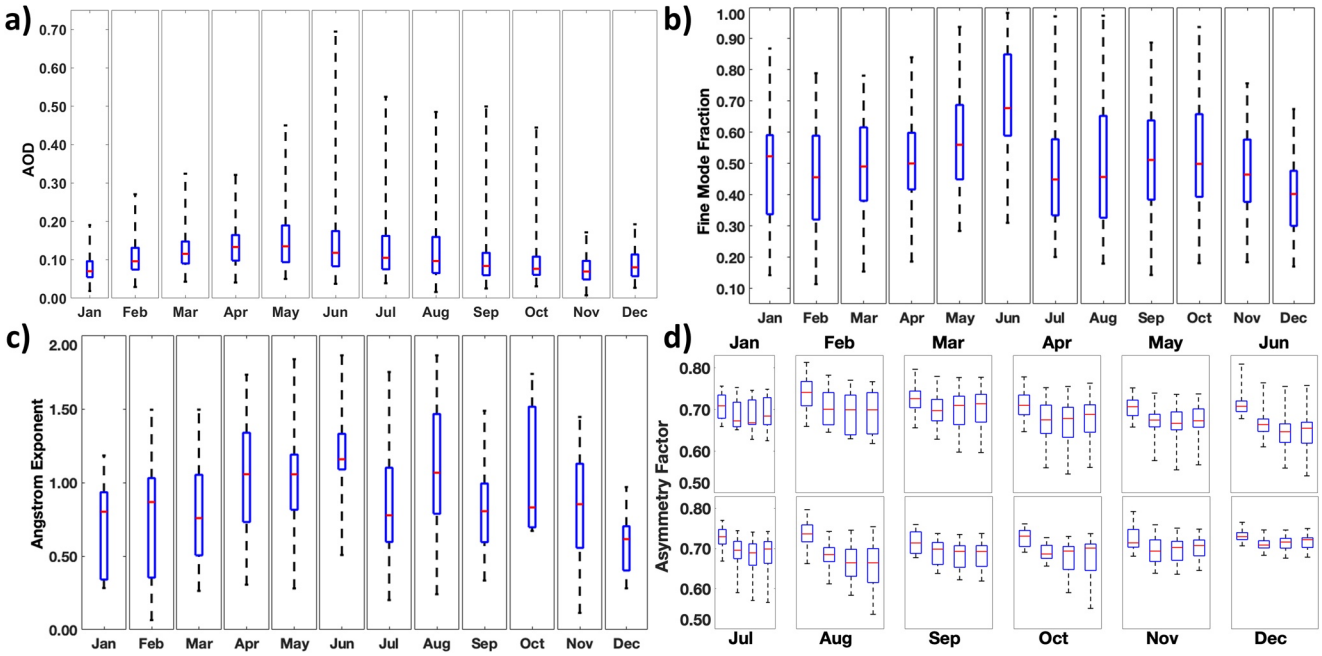

Figure 3. Same as Figure 1 but for AERONET products: (a) AOD, (b) fine mode fraction, (c) Ångström exponent (440/870 nm), and (d) asymmetry factor for 440, 675, 870, and 1020 nm (in order from left to right in each month's panel). Whiskers are the monthly range, red lines represent the median, and the top and bottom of the box represent the 75th and 25th percentile, respectively.

Table 2 provides context for this study's AOD values by comparisons with older studies in Bermuda and other regions. Of note is the global average of 0.12 from the Max-Planck Aerosol climatology (MACv2) (Kinne, 2019), which exactly matches that from the Bermuda AERONET dataset on an annual basis (0.12 ± 0.08). A review of historical ship measurements over various marine regions reported AOD values between 0.07 and 0.12 (Smirnov et al., 2002). Earlier work reported AOD to be 0.14 for Bermuda and 0.13 at Ascension Island, which were nearly twice as high as values for Pacific Ocean island sites owing to frequent influence from smoke, dust, and urban aerosols at the Atlantic sites (Holben et al., 2001; Smirnov et al., 2002). As expected, AOD values are much higher, often exceeding 1, at sites closer to strong pollution sources such as Beijing and in smoke and dust plumes.

3.2.2. Fine Mode Fraction and Ångström Exponent

Fine mode fraction exhibited an annual mean of 0.51 ± 0.18 with relatively similar monthly median values throughout the year (0.40–0.56) with the exception of a higher value in June (0.68) (Figure 3b). The highest single daily was 0.98 (June), whereas the lowest daily value was 0.11 (February). The DJF months exhibited the lowest monthly median values (0.40–0.52), which along with some of the lowest AOD values suggest that there was (i) reduced influence from upwind continental outflow containing fine particles, (ii) more enhanced regional marine emissions (e.g., coarse sea salt), and (iii) reduced hygroscopic growth consistent with the lowest RH values. One way to reconcile the lack of fine particulate pollution and enhanced density of trajectories coming from North America in DJF is that the highest cloud fractions and precipitation occur in DJF over the WNAO (Painemal et al., 2021), and thus there may be extensive wet removal of transported aerosols from North America. MERRA-2 data over the WNAO region (2014–2018) shows that the highest sea salt AOTs occur in DJF and SON, with the lowest values in JJA (Corral et al., 2021), consistent with our FMF results.

The Ångström exponent (AE) parameter provides insight into the size of aerosols, with results expectedly (Eck et al., 2010) pointing to similar features as FMF (Figure 3c). The annual mean value was 0.95 ± 0.39. The maximum monthly median value was in June (1.16) just like FMF, with the highest daily value being 1.86 in that same month. The lowest monthly median values were in DJF (0.62–0.87), whereas MAM (0.76–1.06) and JJA (0.78–1.16) had the highest median values. Values reported in other studies (Table 2) indicate that values

Table 2
Summary of Values for Aerosol Optical Depth, Ångström Exponent, and Asymmetry Factor From This and Other Studies

Region	Aerosol optical depth	References
Bermuda	0.12 ± 0.08	This study
Global average, Max-Planck Aerosol climatology (MACv2)	0.12	Kinne (2019)
Bermuda	0.14	Holben et al., 2001, Smirnov et al. (2002)
Ascension Island	0.13	Smirnov et al. (2002)
Pacific Ocean Islands (Tahiti, Nauru, Lanai)	0.07–0.08	Smirnov et al. (2002)
Bermuda (shipboard measurements)	0.08	Korotaev et al. (1993)
Himalayan Foothills haze event	2.25	Alam et al. (2018)
Zambia, Brazil, Maryland, Moldova smoke episodes	~2	Eck et al. (2003)
Lahore/Karachi (Pakistan) pollution events	> 1	Iftikhar et al. (2018)
Beijing, China	> 1	Bi et al. (2014), Che et al. (2015), Yu et al. (2016)
Indo-Gangetic plains dust storms	> 0.6	Prasad and Singh (2007)
Norway Arctic haze	0.122	Herber et al., 2002
Marine regions, historical ship measurement review	0.07–0.12	Smirnov et al., 2002
	Ångström Exponent	
Bermuda	0.95 ± 0.39	This study
Bermuda	0.93	Smirnov et al. (2002)
Ascension Island	0.6	Smirnov et al. (2002)
Pacific Ocean Islands (Tahiti, Nauru, Lanai)	0.43–0.76	Smirnov et al. (2002)
Remote Atlantic	0.84	Hoppel et al. (1990)
Atlantic air masses	1	Reddy et al. (1990)
North American air masses	1.15	Reddy et al. (1990)
North Atlantic air	0.99	Villevalde et al. (1994)
North Atlantic air: continental polar/maritime arctic/maritime polar	1.27/0.96/1.23	Smirnov et al. (1995)
Kanpur, India	< 0.55 to > 1.1	Eck et al. (2010)
Saharan air masses	0.37 ± 0.18	Reddy et al. (1990)
Smoke air masses	1.1–2.1	Eck et al. (2003)
	Asymmetry factor	
Bermuda	0.72 (440 nm), 0.69 (675 nm), 0.68 (870 nm), 0.68 (1020 nm)	This study
Global average, Max-Planck Aerosol climatology (MACv2)	0.7 (550 nm)	Kinne (2019)
U.S. East coast	0.7 (550 nm)	Hartley and Hobbs (2001)
Saharan dust	0.72–0.73 (500 nm)	Formenti et al. (2000)
Brazil biomass burning	0.54 (550 nm)	Ross et al. (1998)
Central India dust and biomass burning	0.45–0.49 (550 nm)	Jose et al. (2016)
Western, central, and eastern Europe	0.57–0.61 (520–550 nm)	Pandolfi et al. (2018)
Springtime Arctic haze events	0.81 (862 nm)	Herber et al. (2002)
Summer background conditions in Norway	0.62 (862 nm)	Herber et al. (2002)
Western Siberia	0.72 (340 nm), 0.6 (1020 nm)	Zhuravleva et al. (2013)

Table 2
Continued

Region	Aerosol optical depth	References
Lahore, Pakistan	0.78 (440 nm), 0.62 (1020 nm)	Alam et al. (2018)
Karachi, Pakistan	0.74 (440 nm), 0.63 (1020 nm)	Alam et al. (2018)
Tsukuba, Japan	0.585 (550 nm)	Uchiyama et al. (2014)

Abbreviations: DJF, December–January–February; MAM, March–April–May; JJA, June–July–August; SON, September–October–November.

reported here are in general agreement with past measurements over Bermuda and the remote North Atlantic, but in excess of those observed at Pacific Ocean islands (0.43–0.76) and Ascension Island (0.6) (Smirnov et al., 2002). While there was some seasonal variability at Bermuda owing to the shifting relative influence of fine and coarse aerosols (seasonal means ranging between 0.69 [DJF] and 1.05 [JJA]), seasonal differences are not as significant as continental sites closer to emissions sources of anthropogenic fine aerosols and coarse dust such as Kanpur, India (<0.55 to >1.1) (Eck et al., 2010). Values of AE for Saharan air masses are reported to be 0.37 ± 0.18 (Reddy et al., 1990), which is relevant as Saharan air can reach Bermuda especially in summer months when AE values reach as low as 0.20 such as in July. In terms of smoke aerosols, which could possibly reach Bermuda (Mead et al., 2013), past work has shown AE values ranging widely from 1.1 to 2.1 with differences associated with fine mode particle size and contrasting composition (Eck et al., 2003).

Past studies have used a combination of AOD, FMF, and AE values to categorize air masses into types (Che et al., 2015; Kumar et al., 2014, 2015; Pace et al., 2006; Sharma et al., 2014) such as "clean fine" (AOD < 0.1, AE > 1, FMF > 0.7), "polluted fine" (AOD > 0.1, AE > 1, FMF > 0.7), "clean coarse" (AOD < 0.1, AE < 1, FMF < 0.3), and "polluted coarse" (AOD > 0.1, AE < 1, FMF < 0.3) (Sorooshian et al., 2013). Kaskaoutis et al. (2007) defined "desert dust" as occurring when AOD > 0.3 and FMF < 0.6, "clean marine" when AOD < 0.2 and FMF < 0.7, and "urban/industrial" as when AOD > 0.2 and FMF > 0.8. As values in this study fall into intermediate areas not covered by the aforementioned criteria, Bermuda can best be thought of as a "mixed maritime" site as already proposed by Smirnov et al. (2002). While these classifications are based on large dataset statistics, Section 3.4 will demonstrate that Bermuda experiences strong aerosol perturbations that can qualify as either "polluted fine" or "polluted coarse" based on the criteria above.

3.2.3. Asymmetry Factor

The ASY is a critical intensive aerosol property relevant to the aerosol phase function and more broadly for direct aerosol radiative forcing calculations (Andrews et al., 2006; Boucher, 1998; Delene & Ogren, 2002; Russell et al., 1997). Its value describes how well aerosols can scatter light in the forward direction relative to backwards, with values theoretically ranging from −1 (only backscattering) to 1 (only forward scattering) and values of 0 corresponding to uniform scattering. A value of 0.7 is common in radiative transfer models (Pandolfi et al., 2018) and is the global mean reported as part of the MACv2 aerosol climatology (Kinne, 2019). Similar to AE, ASY depends on the size distribution, shape, and composition of aerosols (Pandolfi et al., 2018).

In our analysis, we examine ASY values at four wavelengths (440, 675, 870, 1020 nm) since insights can be gained by comparing different wavelengths (Alam et al., 2014, 2018; Bibi et al., 2016; Yu et al., 2016). Depending on the wavelength, there were varying monthly profiles, with the range in monthly median values being as follows (Figure 3d): 0.71–0.74 with an annual mean of 0.72 ± 0.03 (440 nm), 0.66–0.71 with an annual mean of 0.69 ± 0.04 (675 nm), 0.65–0.72 with an annual mean of 0.68 ± 0.05 (870 nm), 0.66–0.72 with annual mean of 0.68 ± 0.05 (1020 nm). Higher (lower) values were typically observed in DJF (JJA) at the highest wavelengths and especially at 1020 nm. The higher relative contribution of sea salt to the VSDs in DJF (shown in subsequent sections) is consistent with the highest ASY in that season.

Values for Bermuda are fairly similar to those reported for other regions at various wavelengths (Table 2), including 0.7 (550 nm) for the U.S. East Coast (Hartley & Hobbs, 2001). Past studies suggest that a decreasing trend in ASY with increasing wavelength owes to aerosols being predominantly smaller in size (Alam et al., 2014, 2018; Bibi et al., 2016; Yu et al., 2016). The seasonal reduction in median ASY values from 440 to 1020 nm in this study was only 0.02 for DJF, MAM, and SON, whereas it was 0.05 for JJA mostly due to an abnormally high value of 0.74 at 440 nm in August. These reductions are not as pronounced as the previ-

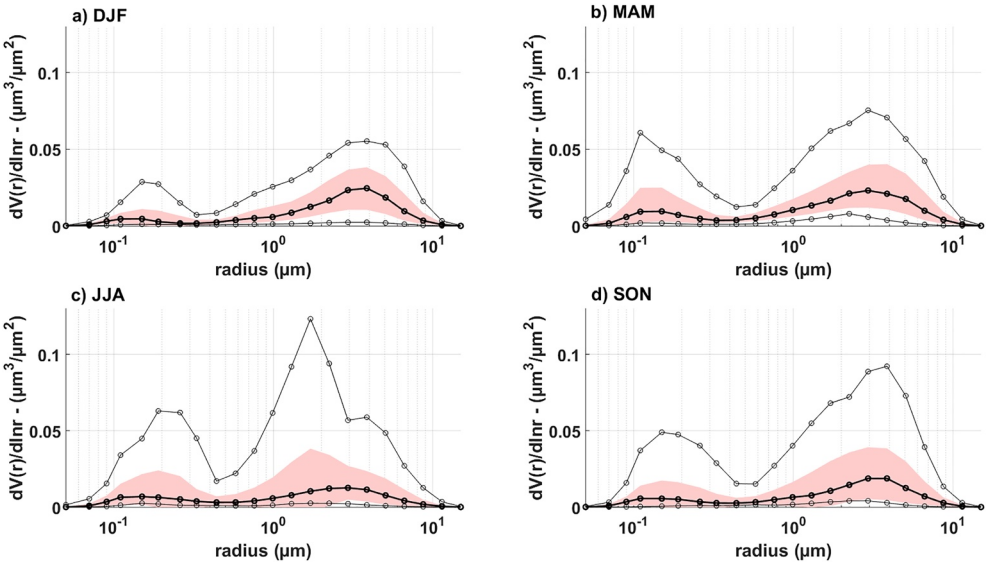

Figure 4. Seasonal volume size distributions based on AERONET data between February 2000 and April 2012. Black curves represent the median, shaded areas represent one standard deviation, and gray curves represent minimum and maximum values. DJF = December–January–February, MAM = March–April–May, JJA = June–July–August, SON = September–October–November.

ously mentioned studies (Alam et al., 2014, 2018; Bibi et al., 2016; Yu et al., 2016), which presumably is due to the higher relative abundance of sea salt at Bermuda compared to sites closer to sources of fine anthropogenic aerosols. At fixed AOD, fine particles have been shown to exhibit lower ASY values as compared to coarse particles (Bi et al., 2014). In addition, Uchiyama et al. (2014) showed that higher ASY values coincide with more contributions from larger particles such as sea salt.

3.2.4. Volume Size Distributions

AERONET provides VSDs using 22 logarithmically equidistant discrete radii between 0.05 and 15 μm. AERONET-based literature recommends a radius of 0.6 μm to separate the fine and coarse modes (Dubovik et al., 2002; Schuster et al., 2006). Seasonal VSDs were bimodal on average with peaks in both the fine and coarse modes (Figure 4). Although the median distributions show one pronounced peak in volume concentration in both the fine and coarse modes, the two modes were quite broad suggestive of numerous sources. During DJF and SON, the most prominent fine and coarse mode peaks occurred at radii of 0.11–0.15 and 3.86–5.06 μm, respectively, with associated median total/fine/coarse volume concentrations being 0.05/0.01/0.04 and 0.04/0.01/0.03 $\mu m^3\ \mu m^{-2}$. For both MAM and JJA, the fine mode peak was similarly between 0.11 and 0.15 μm but with the coarse mode peak shifted to smaller sizes (2.24–2.94 μm). The highest median volume concentrations of any season were during MAM, with total/fine/coarse values being 0.06/0.01/0.04 $\mu m^3\ \mu m^{-2}$. The JJA season exhibited median total/fine/coarse volume concentrations of 0.04/0.01/0.02 $\mu m^3\ \mu m^{-2}$.

Table 3
Seasonal Median Values of Fine and Coarse Mode Characteristics, Including Volume Concentration (V, $\mu m^3\ \mu m^{-2}$), Effective Radii (R_{eff}, μm), Volume Median Radii (R, μm), and Geometric Standard Deviation (σ)

	Fine mode				Coarse mode			
Season	V_f	$R_{eff\text{-}f}$	R_f	σ_f	V_c	$R_{eff\text{-}c}$	R_c	σ_c
DJF	0.01	0.14	0.17	0.51	0.04	2.08	2.64	0.69
MAM	0.01	0.14	0.16	0.47	0.04	1.88	2.43	0.69
JJA	0.01	0.16	0.17	0.45	0.02	1.85	2.37	0.68
SON	0.01	0.15	0.17	0.50	0.03	2.09	2.72	0.66

Abbreviations: DJF, December–January–February; MAM, March–April–May; JJA, June–July–August; SON, September–October–November.

Table 3 compares size distribution parameters for the fine and coarse modes, including effective radius (R_{eff}: ratio of average radius weighted by geometrical cross-sectional area), volume median radius (R: mean logarithm of the radius), and geometric standard deviation (σ). There was minimal variability in R_{eff} and R for the fine mode, with seasonal median values ranging from 0.14 – 0.16 μm and 0.16–0.17 μm, respectively. The width of the fine mode distribution was broadest for DJF ($\sigma = 0.51$) and SON ($\sigma = 0.50$), in contrast to MAM (0.47) and JJA (0.45). For the coarse mode, there was more seasonal variability in R_{eff} (1.85–2.09 μm) and R (2.37–2.72 μm), and slightly less variability in σ (0.66–0.69).

The DJF season exhibited the least amount of variability as the standard deviation in volume concentrations (total/fine/coarse) was the lowest of any season and the range between the minimum and maximum concentrations for all three categories (total/fine/coarse) was the lowest (0.10/0.03/0.10 $\mu m^3\ \mu m^{-2}$). This suggests that the DJF season has the least influence from episodic intrusions of aerosol types such as smoke, dust, and continental urban pollution. As previously discussed, DJF was relatively more influenced by regional emissions in the form of sea salt and potentially other forms of marine-derived emissions such as oxidation products from dimethylsulfide like sulfate and methanesulfonic acid (Sorooshian et al., 2015; Wadleigh, 2004). The shift in the coarse mode peak, in addition to R_{eff} and R, to smaller sizes in MAM and JJA may be reflective of the characteristic size of dust aerosol reaching Bermuda. Distinct coarse mode peaks for dust and sea salt become evident by comparing VSDs for MAM, SON, and JJA. There is a peak in the 2.94–3.86 μm range, similar to DJF, likely due to the background sea salt present in the region. Past work for Bermuda showed that sea salt mass typically peaks in the size fraction between 3.2 and 5.6 μm (Keene et al., 2007). In addition, there is a separate peak for all three seasons at 1.71 μm, which presumably represents dust. As the dust impacting Bermuda was transported much farther than sea salt, it is plausible that the characteristic dust peak is at a smaller size than sea salt. This is supported by past studies: (i) African dust reaching Miami, Florida exhibits most of its mass at geometric diameters below 2.1 μm (Kramer et al., 2020); and (ii) mass mean diameters of African dust are less than 1 μm by the time they reach the U.S. East Coast (Perry et al., 1997), which can take approximately a week of transport time (Carlson & Prospero, 1972).

For context, VSD characteristics in this study are compared to other regions. In their analysis of various maritime regions, Smirnov et al. (2002) observed a characteristic bimodal lognormal size distribution with modes centered at effective radii of 0.11 μm and either 2.3 μm (Pacific Ocean) or 1.9 μm (Atlantic Ocean). Larger radii for the fine mode have previously been linked to conditions of greater plume age allowing for more coagulation and condensational growth (Eck et al., 2003); results for Bermuda do not indicate fine mode radii that are especially large or different between seasons that have varying predominant air mass source origins (Figure 1). Cases of smoke in various regions have revealed fine mode radii ranging between 0.17 and 0.25 μm with a less prominent coarse mode (Eck et al., 2003); that study reported variability in the radii to be due to varying fuel types, combustion condition, and age of plumes. Aside from smoke conditions, other cases of fine mode concentrations exceeding that of the coarse mode include megacities like Beijing with extensive amounts of urban pollution (Che et al., 2015); however, in those types of megacities the coarse mode volume can at times exceed that of the fine mode owing to sources such as fly ash and fugitive dust emissions (Eck et al., 2005). Fine and coarse mode concentrations were reported to be 0.12 and 0.14 $\mu m^3\ \mu m^{-2}$, respectively, for dust transported over Beijing in January 2013 (Yu et al., 2016). Dusty days over the Middle East and Southwest Asia exhibited peak volume concentrations at radii of 1.70 and 2.24 μm (Alam et al., 2014), overlapping with where the presumed dust peak is in our study. Dust over the Indo-Gangetic plains exhibited peaks in the VSD at 1.71–2.24 μm, but with much higher peaks than Bermuda reaching values as high as 0.99 $\mu m^3\ \mu m^{-2}$ (Prasad & Singh, 2007). Another study focused on the Indo-Gangetic plains observed coarse mode volume concentrations of 0.4–0.5 $\mu m^3\ \mu m^{-2}$ during dust transport periods as compared to 0.1–0.2 $\mu m^3\ \mu m^{-2}$ at other times (Dey et al., 2004). That study and others (Alam et al., 2018; Che et al., 2015; Smirnov et al., 2002) pointed to both additional VSD modes and enhanced overall volume concentrations due to hygroscopic growth of particles at enhanced RHs.

While this study is focused on monthly and seasonal scales, future work is warranted to examine effects better resolved at finer temporal scales such as those of cloud processing and wet scavenging on the VSDs at Bermuda. Eck et al. (2012) showed that cloud processing can yield a larger accumulation mode peak around radii of ~0.4–0.5 μm in addition to a typical smaller peak at ~0.12–0.20 μm. As the atmospheric column above Bermuda is impacted by clouds throughout the year, it is very likely that cloud processing impacts aerosol volume concentrations. The winter has the highest cloud cover over the WNAO (Painemal et al., 2021) and would be most ideal to extract a cloud processing signature in aerosol properties. September and October are the months featuring the most intense rainfall (Figure 2c) and are excellent candidate months for observing scavenging effects. Furthermore, vertically resolved measurements with airborne platforms would be of great value as significant changes were reported over 30 years ago below and above 0.5 km; more specifically, the geometric mean diameter of number/volume changed from 0.84/3.3 μm at high altitude (>0.5 km) to 2.16/5.12 μm at low altitude (Horvath et al., 1990). Moreover, that study showed

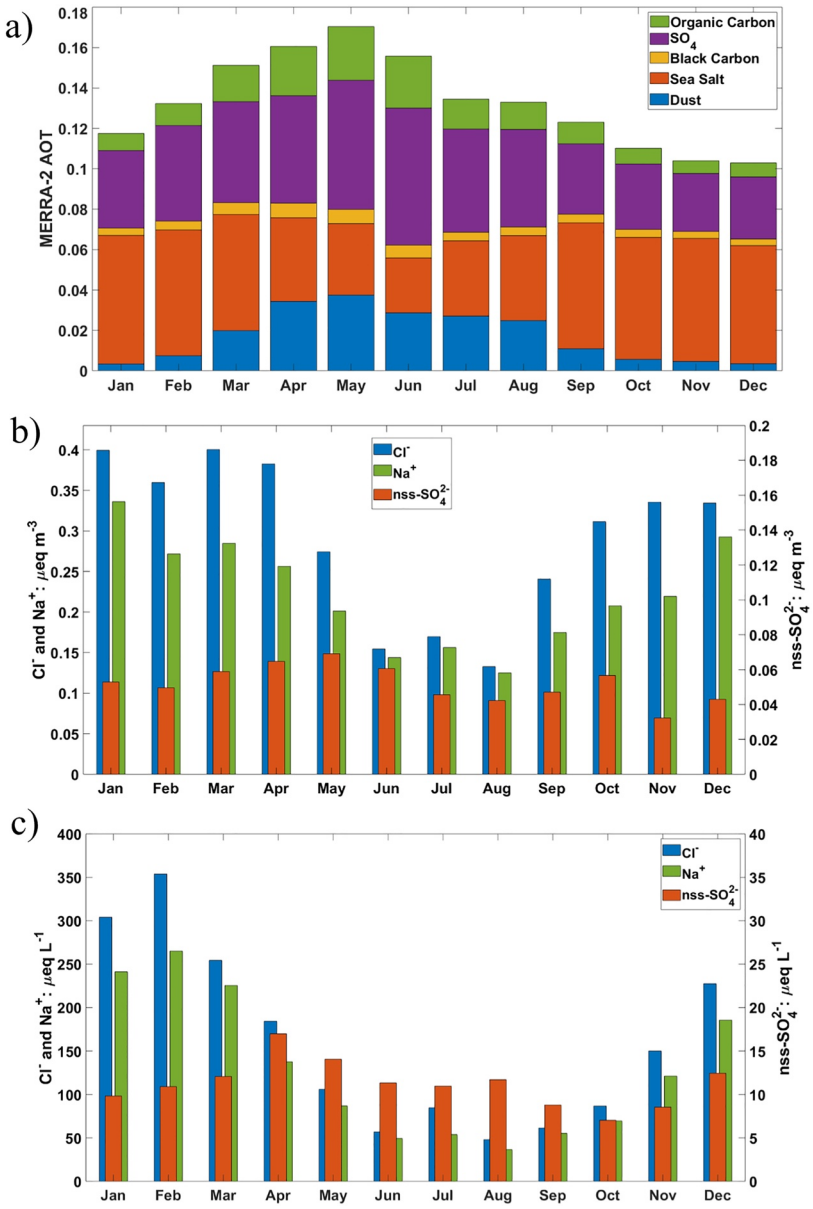

Figure 5. Monthly mean values of composition data: (a) MERRA-2 speciated AOT (550 nm) for dust, sea salt, black carbon, sulfate, and organic carbon; and surface measurements of Cl^-,Na^+, and nss SO_4^{2-} in (b) aerosol and (c) wet deposition samples collected at Fort Prospect.

that number and volume concentrations were enhanced by one and two orders of magnitude, respectively, at low altitude. A separate study independently confirmed much lower volume concentrations in the free troposphere (0.13 μm^3 μm^{-3}) over Bermuda versus the marine boundary layer (0.74 μm^3 μm^{-3}) (Kim et al., 1990). There clearly are important vertical features that surface observations alone cannot identify and Section 3.2.6 will expand on this issue.

3.2.5. Composition

Monthly mean values of MERRA-2 speciated AOT for five major aerosol components (organic carbon, sulfate, black carbon, sea salt, dust) are summarized in Figure 5a. For most of the year (September–March), sea salt accounted for the highest AOT values (38%–59% of total) ranging in monthly mean values between 0.058 and 0.064. The second most abundant component in those same months (September–March) was sulfate (0.029–0.050; 28%–33%) followed by either organic carbon or dust, and then black carbon. Sea

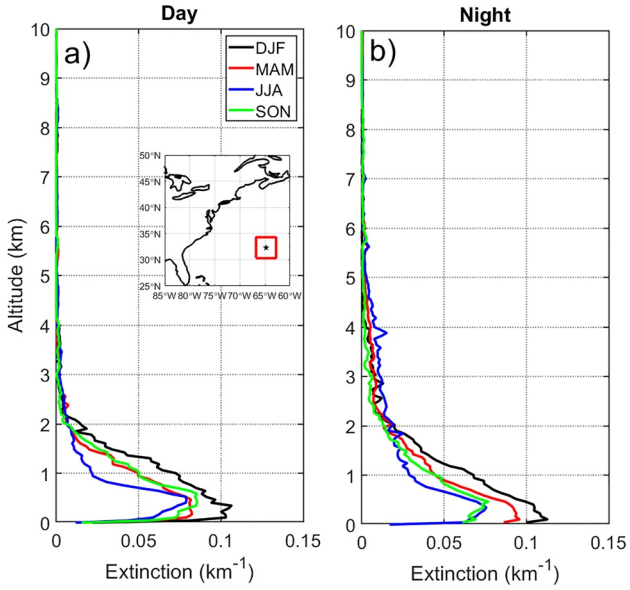

Figure 6. Vertical distribution of mean aerosol extinction (532 nm) from CALIOP's (a) daytime and (b) nighttime observations over a 4 ° × 4 ° domain (see inset map) surrounding Bermuda based on data between June 2006 and December 2012.

salt was unique in its annual cycle with higher AOT values in the colder months, whereas the other species were most enhanced between April and August. Between April and August, sulfate accounted for the highest monthly mean AOT values (0.048–0.068; 33%–44%) assisted in part by conditions that promote secondary formation such as increased solar radiation and humidity. The same reasons can plausibly be linked to the enhancement of organic carbon in those same months (0.013–0.024; 10%–15%), with an additional reason potentially being influences from biomass burning plumes enriched with organic carbon (Reid et al., 2005). This is supported by how black carbon exhibited its highest AOTs between April and June (0.006–0.007; 4%). Lastly, dust showed its highest AOT values between March and August (0.020–0.037; 13%–22%), with the peak value in May.

In situ aerosol and wet deposition composition data collected at Fort Prospect show monthly trends matching those of MERRA-2 for the three species examined (Cl^-, Na^+, nss SO_4^{2-}) (Figures 5b and 5c). Specifically, the sea salt tracer species peak in their concentrations in DJF, with monthly mean aerosol/wet deposition values of Cl^- and Na^+ ranging from 0.33-0.40 μEq m^{-3}/228–354 μEq L^{-1} and 0.27-0.34 μEq m^{-3}/186–265 μEq L^{-1}, respectively. Minimum concentrations of those two species occurred in JJA with monthly mean concentrations of aerosol Cl^- and Na^+ ranging from 0.13 to 0.17 μEq m^{-3} and 0.13 to 0.16 μEq m^{-3}, respectively, and wet deposition Cl^- and Na^+ values ranging from 48 to 85 and 37 to 54 μEq L^{-1}, respectively. There was a less pronounced annual cycle for nss SO_4^{2-}, with the exception of higher values in MAM when monthly mean concentrations ranged from (aerosol) 0.06 to 0.07 μEq m^{-3} and (wet deposition) 12 to 17 μEq L^{-1}. The annual mean ratio between nss SO_4^{2-} and the combined sum of Cl^- and Na^+ was 11% and 5% for aerosol and wet deposition samples, respectively, which is much less than what is depicted by MERRA-2. This may be in part due to the columnar nature of MERRA-2 AOT data as compared to the aerosol and wet deposition samples, suggesting potentially that there is considerable SO_4^{2-} above the PBLH relative to sea salt.

It is worth noting that a separate dataset for wet deposition composition was collected over Bermuda at Tudor Hill (64.87° W, 32.27° N) covering the time period between January 1989–February 1997 and July 2006–June 2009, including the following ions (Keene et al., 2014): Na^+, Cl^-, Ca^{2+}, Mg^{2+}, K^+, NH_4^+, NO_3^-, SO_4^{2-}. A recent analysis of that dataset revealed that the combined contribution of Na^+ and Cl^- to the total ion concentration measured was ~83% for the cumulative time period, with the highest volume-weighted concentrations in DJF (Ma et al., 2021). Monthly mean mass fractions of sea salt varied between 86% and 97%, with the next most abundant ions being nss SO_4^{2-} (1%–4%) and NO_3^- (≤3%), the latter two of which contributed more between May and September. Earlier work also showed greater wet deposition of SO_4^{2-} and NO_3^- in summer months (Moody & Galloway, 1988). Those results are consistent with the Fort Prospect data.

The composition data support that there is contrasting composition throughout the year based on air mass transport patterns and varying meteorological conditions. These results also validate speculations in previous sections (3.2.2–3.2.4) about sea salt being most prominent in DJF without other major sources as that season exhibited the lowest AOD, FMF, and AE values, along with the highest ASY value and among the higher coarse mode volume concentration, R_{eff}, and R values. An implication of these results is that aerosol-based studies desiring conditions more reflective of a marine natural background are best suited for the winter season whereas those targeting perturbations from continental regions are best suited for spring and summer months.

3.2.6. CALIOP Vertical Profiles

Mean aerosol extinction vertical profiles are shown in Figure 6 across various seasons for both daytime and nighttime conditions. The common feature in all extinction profiles is the occurrence of maximum extinction in the levels near the surface, followed by a sharp decrease at higher altitudes. This is consistent with

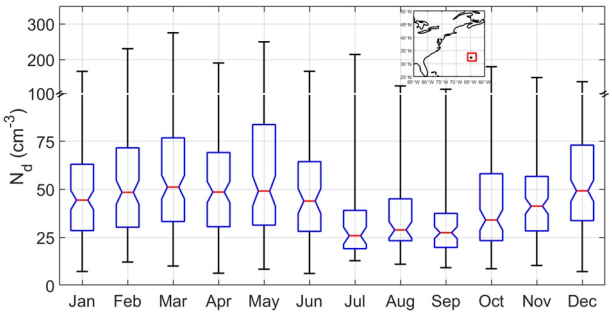

Figure 7. Monthly statistics associated with cloud droplet number concentration (N_d) as derived from CERES-MODIS data surrounding Bermuda (31–34°N; 63–66°W; red box in inset map) between 2013 and 2017. Whiskers are the monthly range, red lines represent the median, and the top and bottom of the box represent the 75th and 25th percentile, respectively. The notches in the box plots demonstrate whether medians are different with 95% confidence.

previous reports of major reductions in the aerosol number and volume concentrations above the surface and into the free troposphere above Bermuda (Horvath et al., 1990; Kim et al., 1990).

The DJF season generally exhibited the highest extinction values with a maximum nighttime average value of 0.112 km^{-1} (0.106 km^{-1} for daytime profile) at 0.10 km altitude (0.34 km for daytime) followed by a decline to 0.02 km^{-1} at 2.08 km (1.78 km for daytime). Based on the results already presented, sea salt is largely responsible for the appreciable extinction values in DJF at low altitude. In contrast, JJA had the lowest extinction values in the bottom 2 km with a maximum nighttime average extinction value of 0.076 km^{-1} (0.079 km^{-1} for daytime profile) at 0.34 km (0.46 km for daytime). Vertical aerosol extinction profiles for MAM and SON were intermediate to those of DJF and JJA in the bottom 2 km.

CALIOP's nighttime observations are known to have better data quality than daytime due to improved signal-to-noise ratio in the absence of sunlight (Tackett et al., 2018; Winker et al., 2009). An interesting feature revealed by nighttime profiles is that JJA exhibits slightly greater mean extinction values above 2.26 km as compared to the other seasons. This is most likely due to the advection of African dust plumes in JJA, although there could be influence from urban pollution and smoke. Nighttime mean AOD values, obtained from integrating CALIOP vertical extinction profiles, are 0.146, 0.128, 0.114, and 0.100 (0.135, 0.101, 0.078, and 0.103 for daytime) for DJF, JJA, MAM, and SON, respectively. There is disagreement when comparing the extinction profiles and AOD values derived from CALIOP observations with MERRA-2 and AERONET results shown earlier. For instance, CALIOP aerosol values are highest in DJF; in contrast, those months have the lowest MERRA-2 AOT and AERONET AOD values. This may be linked to a combination of the limitation of CALIOP to detect faint aerosol layers in the atmosphere and the different spatial extents associated with AERONET, CALIOP, and MERRA-2.

3.3. Cloud Droplet Number Concentration

Aerosols serve as cloud condensation nuclei (CCN) and directly impact cloud droplet number concentrations (N_d), which is an important cloud microphysical property impacting cloud albedo and precipitation characteristics. Consequently, aerosol results described up to now have direct implications for values and the seasonal cycle of N_d. The notched box plot format of Figure 7 shows that the amplitude of the seasonal N_d cycle is statistically significant (95% confidence). The MAM and DJF seasons exhibited the highest monthly median N_d values ranging from 55 cm^{-3} (April) to 63 cm^{-3} (May) and from 52 cm^{-3} (January) to 59 cm^{-3} (February), respectively. Minimum seasonal N_d values were in JJA and SON with monthly median ranges of 36–51 cm^{-3} and 33–47 cm^{-3}, respectively. The maximum single day N_d value of 275 cm^{-3} was observed in March, whereas the monthly minimum N_d values ranged between 6 and 13 cm^{-3}. These results highlight the discrepancy between monthly profiles of AERONET AOD and MERRA-2 AOT versus N_d in the region as among the lowest (highest) values of AOD (N_d) that occur in the same season of DJF. Although the nighttime mean AOD values from CALIOP were highest in DJF, there was a high sea salt presence (Section 3.2.5) that is not necessarily indicative of high aerosol number concentrations.

Differences between the aerosol products and N_d are the subject of forthcoming work and are hypothesized to be due at least partly to some combination of the following factors: aerosol size distribution, vertical distribution of aerosol, humidity effects, stronger aerosol–cloud interactions in DJF, and assumptions in N_d retrievals. To elaborate on some of these factors, AOD can be biased high without a proportional increase in N_d if there are fewer but larger particles (e.g., salt and dust-rich air masses vs. sulfate -rich plumes) and if it is especially humid leading to particle hygroscopic growth (which does not change number concentration but rather particle size and thus AOD). Furthermore, the vertical aerosol distribution is significant as aerosol layers above clouds will influence AOD but not necessarily N_d.

Table 4
Summary of Data Values on extreme AOD Days Based on Criteria Presented in 2.2

		AERONET		MERRA-2					
Date	Aerosol Type	AOD	FMF	Dust	SS	BC	SO4	OC	Total
26-Feb-2000	N. America Urban Outflow	0.27	0.70	0.01	0.06	0.00	0.15	0.01	0.23
26-May-2002	N. America Urban Outflow	0.41	0.77	0.03	0.04	0.01	0.14	0.04	0.26
21-Jun-2011	N. America Smoke Outflow	0.69	0.91	0.02	0.05	0.02	0.09	0.17	0.35
02-Sep-2010	African Dust	0.50	0.18	0.25	0.10	0.00	0.04	0.01	0.41

Note. Shown are the daily average values of AERONET AOD and fine mode fraction (FMF), the predominant aerosol type based on NAAPS and MERRA-2 data, MERRA-2 total and speciated AOT (sea salt = SS, black carbon = BC, organic carbon = OC).

Of relevance to interrelationships between aerosol and N_d data is the interpretation of wet deposition composition data at Bermuda (Section 3.2.5), which indicates what aerosol types serve as CCN in clouds, since those drops eventually can grow to become sufficiently large to fall as rain drops to the surface. The wet deposition data suggest that sea salt is influential in cloud microphysical processes year-round at Bermuda, and especially in the winter season, which is consistent with aerosol data in previous sections showing that sea salt is most prominent in winter. It is unclear though as to how significant sea salt is seasonally relative to other aerosol types in terms of overall CCN number concentration. This is because the number concentration of sea salt might be low in contrast to its mass concentration based on its large size. Future work is needed to answer the question as to the relative importance seasonally of different aerosol types such as sea salt, dust, and secondarily formed aerosols in terms of CCN number concentration. This is especially interesting for DJF when N_d values are relatively high, which raises the question as to whether this is due to enhanced sea salt rather than transported urban continental outflow, a case of which is profiled in the next section. The interaction of different CCN types is an interesting question since depending on the amount of cloud liquid water and N_d range, large drops formed from coarse salt particles can expedite the broadening of droplet size spectra in clouds to promote rain (Blyth et al., 2003; Dadashazar et al., 2017; Feingold et al., 1999; Jung et al., 2015).

Low-level liquid clouds over Bermuda are exceptionally clean when contrasted with other regions. For regional context, monthly mean N_d values derived from AQUA-MODIS over the WNAO region range from as low as ~90 cm^{-3} in July to ~165 cm^{-3} in January (Sorooshian et al., 2019), whereas the annual mean and standard deviation at Bermuda in this study is 51.3 ± 1.7 cm^{-3}. In a review of stratocumulus clouds, Wood (2012) stated that N_d can range from being less than 10 cm^{-3} in "extremely aerosol-rare conditions" over the oceans to reaching over 500 cm^{-3} in more polluted conditions. Furthermore, higher N_d values (>200 cm^{-3}) were noted to be a common downwind of continents, while lower values (≤50 cm^{-3}) are more common over remote ocean areas and especially in the tropics and sub-tropics. In a review of 13 years of AQUA-MODIS warm cloud N_d data across the global ice-free oceans, mean values across the globe ranged from 45.4 to 240 cm^{-3} (Bennartz & Rausch, 2017). Over the Southern Ocean, which is thought to be a relatively cleaner region of the world, values between 100 and 200 cm^{-3} were recently observed (Chubb et al., 2016). The relatively low N_d values at Bermuda present important opportunities for aerosol–cloud investigations aiming to obtain statistics in a region with low N_d conditions, but with the advantage of aerosol perturbations on cloud properties in the form of episodic plumes of dust, smoke, and anthropogenic emissions.

3.4. Extreme Aerosol Events

This section focuses on high pollution events based on AERONET AOD with the intent to summarize characteristic aerosol parameter values and source regions causing the events. Following the criteria in Section 2.2, one extreme event is profiled per season and summarized in Table 4 and Figure 8. The combination of AERONET, NAAPS, MERRA-2, and HYSPLIT is used to identify sources, transport corridors, and relevant aerosol characteristics for each event. We use ending altitudes of both 0.5 and 3 km for HYSPLIT

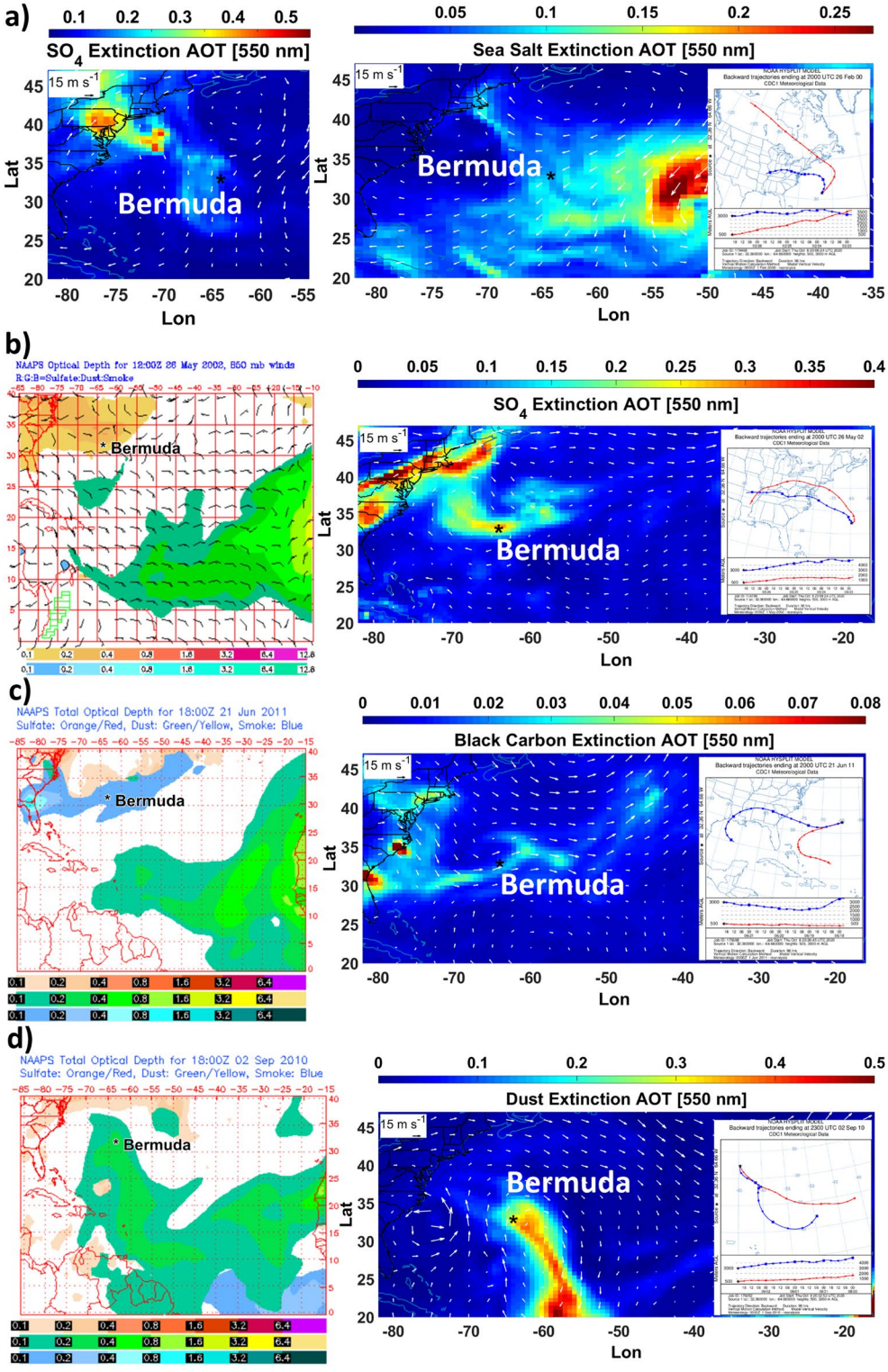
a)
SO4 Extinction AOT [550 nm]
Sea Salt Extinction AOT [550 nm]
15 m s-1
Bermuda
Lat
Lon
b)
NAAPS Optical Depth for 12:00Z 26 May 2002, 850 mb winds
R:G:B=Sulfate:Dust:Smoke
SO4 Extinction AOT [550 nm]
c)
NAAPS Total Optical Depth for 18:00Z 21 Jun 2011
Sulfate: Orange/Red, Dust: Green/Yellow, Smoke: Blue
Black Carbon Extinction AOT [550 nm]
d)
NAAPS Total Optical Depth for 18:00Z 02 Sep 2010
Sulfate: Orange/Red, Dust: Green/Yellow, Smoke: Blue
Dust Extinction AOT [550 nm]

trajectories over Bermuda to represent boundary layer and free tropospheric layers, respectively, based on PBLHs shown in Figure 2d.

The event representing the DJF season occurred on 26 February 2000 (Figure 8a) and was the highest AOD event of that season in the full dataset (0.27). The HYSPLIT back-trajectories show the influence of a North American air mass that subsided from 4 to 0.5 km over the four days prior to reaching Bermuda. The trajectory ending at 3 km stayed mostly between 3 and 4 km. MERRA-2 wind data are consistent with North American outflow, which likely impacted the column of air above the island in addition to local marine emissions as wind speeds at 975 hPa were fairly high in proximity to Bermuda (~10–15 m s^{-1}; 62.5–65°W, 32–34°N). The FMF value was 0.70, indicative of the enhanced influence of fine aerosols. This is consistent with the speciated AOT from MERRA-2 being highest for sulfate (0.15) among all five species. In contrast, organic carbon, black carbon, and dust individually exhibited AOTs ≤ 0.01, and sea salt had an AOT of 0.06. Therefore, this is a case presumed to have influence from both North American pollution enhanced with sulfate and also sea salt.

The event chosen for MAM occurred on 26 May 2002 (Figure 8b) and was categorized as having influence from North American continental outflow with a strong sulfate signature derived from urban emissions. Similar to the last case, there was evidence of relatively high concentrations of fine aerosols (FMF = 0.77) and with the air mass being transported aloft (~1.5 km) before subsiding down to 0.5 km over Bermuda. The trajectory ending at 3 km was transported between 3 and 5 km. This day coincided with the fourth-highest AERONET AOD (0.41) of the MAM season for the full study period. Interestingly, the following day exhibited an AOD of 0.44. MERRA-2 AOT data reveal that sulfate's value was highest on the 26th (0.14) whereas the other speciated AOT values were ≤0.04. Both NAAPS and MERRA-2 show that high sulfate levels were present along most of the U.S. East Coast.

The summer event on 21 June 2011 demonstrates an example of how a biomass burning plume stemming from the continental U.S. reaches Bermuda (Figure 8c). There were fire hotspots across the southeast U.S. and the mid-Atlantic area of the U.S. East Coast as confirmed by NAAPS, MERRA-2, and fire data from the Fire Information for Resource Management System (FIRMS), which uses active fire data from MODIS and the Visible Infrared Imaging Radiometer Suite (VIIRS). This was the highest AOD day (0.69) of any season. The FMF was 0.91, which is a value consistent with other smoke studies reporting a high presence of fine aerosols (Che et al., 2015; Salinas et al., 2013). While the HYSPLIT back-trajectory ending at 0.5 km was transported within the bottom 0.5 km in the previous four days and did not come from the continental U.S., the trajectory ending at 3 km came from the smoke-rich areas over the U.S. indicating that the smoke was in the free troposphere over Bermuda. MERRA-2 estimated that the organic carbon AOT was most dominant (0.17) on this day, consistent with this species being enhanced in biomass burning plumes. Black carbon AOT was 0.02, which was among the highest values during the study period over Bermuda. Sulfate AOT was 0.09, while dust and sea salt AOTs were 0.02 and 0.05, respectively.

The last event occurring on 2 September 2010 (Figure 8d) shows the influence of an African dust plume as confirmed by NAAPS, MERRA-2, and HYSPLIT. This event is characterized by the fourth highest AOD (0.50) of the study period with the subsequent day (3 September 2010) having an AOD of 0.38. The FMF value on 2 September was 0.18, which dropped slightly to 0.16 the subsequent day. MERRA-2 estimated that dust had the highest speciated AOT (0.25) followed by sea salt (0.10), sulfate (0.04), and then organic carbon (0.01) and black carbon (0.00). Therefore, the very low FMF value on 2 September was not just from dust but also from significant local sea salt influence, which is supported by the strong winds at 975 hPa around Bermuda (~15–20 m s^{-1}; 62.5–65°W, 32–34°N).

Figure 8. Case studies of extreme events: (a) sulfate plume from North America on 26 February 2000; (b) sulfate plume from North America on 26 May 2002; (c) biomass burning plume from North America on 21 June 2011; and (d) African dust plume on 2 September 2010. Shown are spatial maps of speciated AOD from NAAPS and AOT from MERRA-2 (2100 UTC), in addition to HYSPLIT back-trajectories ending at 0.5 and 3 km over Bermuda. Superimposed on the MERRA-2 maps are wind data (700 hPa) at 2100 UTC, which is representative of an altitude aloft where pollution is transported; those data were expanded from the native spatial resolution (0.5 ° × 0.625 °) to coarser resolution (2.0 ° × 2.5 °) using bilinear interpolation. The winds on the sea salt panel of (a) are at 975 hPa to represent near-surface conditions. NAAPS data were unavailable for the year 2000 and are not shown in (a).

4. Conclusion

This work uses multiple years of data from observational platforms and models to present a detailed aerosol climatology for a remote island (Bermuda) over the western North Atlantic Ocean exposed to long-range transport from multiple continents. Aerosol data are examined in relation to meteorology, atmospheric circulation, cloud droplet number concentrations, and wet deposition composition. Mean annual values are as follows for AERONET parameters: AOD = 0.12 ± 0.08, FMF = 0.51 ± 0.18, Ångström exponent = 0.95 ± 0.39, ASY = 0.72 ± 0.03 (440 nm) to 0.68 ± 0.05 (1020 nm). VSDs were bimodal with more volume concentrated in the coarse mode. Effective radii in the fine and coarse modes varied between 0.14–0.16 and 1.85–2.09 μm, respectively. Volume size distribution data suggest that dust exhibits a smaller characteristic size than sea salt, with the former mode most evident in the summertime when African dust regularly reaches Bermuda. Important seasonal changes are evident including more sea salt influence in the winter (DJF) and fall (SON), and greater influence from other aerosol species (e.g., dust, sulfate, organic carbon, black carbon) in spring (MAM) and summer (JJA). MERRA-2 data reveal that sea salt exhibits the highest AOT values between September and March, with the peak in relative contribution in DJF coinciding with the following features: lowest seasonal values of AOD, FMF, and Ångström exponent; least variability in VSDs; highest ASY; highest aerosol extinction values in the bottom 2 km; highest aerosol and wet deposition concentrations as measured at the surface. The summer months showed enhanced aerosol extinction values above 2.25 km due largely to transported dust.

Bermuda is shown to represent a location that has generally "clean clouds", which is common for a remote marine region. The mean annual cloud droplet number concentration value was 51.3 cm^{-3}, with DJF and MAM exhibiting the highest monthly median values (52–63 cm^{-3}) and JJA and SON having a range of 33–51 cm^{-3}. Daily values can reach as high as 275 cm^{-3} though, pointing to the influence of strong aerosol perturbations resulting from transported plumes. Sea salt is a major year-round source of CCN based on how it dominates ionic composition in wet deposition collected on the island. It is unclear why cloud droplet number concentration and AOD exhibit different annual cycles, and this will be the subject of forthcoming work.

This study shows that Bermuda not only represents a remote marine site with extensive sea salt influence, but is vulnerable to continental emissions that undergo long-range transport that can either remain aloft or entrain down to impact the boundary layer. Examples are shown of extreme AOD events linked to North American urban and smoke outflow in addition to an African dust plume. In this regard, it is an intriguing area to conduct aerosol–cloud interaction investigations as strong aerosol perturbations occur periodically superimposed on the background marine signature comprising sea salt and other ocean-derived aerosol species such as sulfate, methanesulfonic acid, and secondary organic aerosol. While it is of interest to see how these perturbations impact cloud properties, another intriguing avenue of research is to study how clouds impact aerosols via cloud processing and wet scavenging. Furthermore, it is of interest to conduct similar types of analyses at other remote marine sites over the Atlantic Ocean (e.g., Ascension Island) and other ocean basins (e.g., Lanai, Midway, Tahiti, Kaashidhoo, Darwin) (Ahmad et al., 2010) to determine how representative the results for Bermuda are for a remote marine location.

Data Availability Statement

Data used in this study are publicly available at the websites provided in Section 2.

Acknowledgments
This research was funded by NASA Grant 80NSSC19K0442 in support of the ACTIVATE Earth Venture Suborbital-3 (EVS-3) investigation, which is funded by NASA's Earth Science Division and managed through the Earth System Science Pathfinder Program Office. The AERONET station in Bermuda is maintained on behalf of NASA by the Bermuda Institute of Ocean Sciences at the Tudor Hill Marine Atmospheric Observatory, which is currently supported by NSF award 1829686, and by previous such awards during the time period in this study. Aerosol and wet deposition chemistry data at Fort Prospect are from the Bermuda Air Quality Program, operated by BIOS with funding from the Department of Environment and Natural Resources, Government of Bermuda. The authors acknowledge the NOAA Air Resources Laboratory (ARL) for the provision of the HYSPLIT transport and dispersion model and READY website (http://ready.arl.noaa.gov) used in this work. The authors acknowledge the use of data and imagery from LANCE FIRMS operated by NASA's Earth Science Data and Information System (ESDIS) with funding provided by NASA Headquarters.

References

Ahmad, Z., Franz, B. A., McClain, C. R., Kwiatkowska, E. J., Werdell, J., Shettle, E. P., & Holben, B. N. (2010). New aerosol models for the retrieval of aerosol optical thickness and normalized water-leaving radiances from the SeaWiFs and MODIS sensors over coastal regions and open oceans. *Applied Optics*, *49*(29), 5545–5560. https://doi.org/10.1364/Ao.49.005545

Alam, K., Khan, R., Sorooshian, A., Blaschke, T., Bibi, S., & Bibi, H. (2018). Analysis of aerosol optical properties due to a Haze episode in the Himalayan foothills: Implications for climate forcing. *Aerosol and Air Quality Research*, *18*(5), 1331–1350. https://doi.org/10.4209/aaqr.2017.06.0222

Alam, K., Trautmann, T., Blaschke, T., & Subhan, F. (2014). Changes in aerosol optical properties due to dust storms in the middle east and southwest Asia. *Remote Sensing of Environment*, *143*, 216–227. https://doi.org/10.1016/j.rse.2013.12.021

Aldhaif, A. M., Lopez, D. H., Dadashazar, H., & Sorooshian, A. (2020). Sources, frequency, and chemical nature of dust events impacting the United States East Coast. *Atmospheric Environment*, *231*, 117456. https://doi.org/10.1016/j.atmosenv.2020.117456

Anderson, J. R., Buseck, P. R., Patterson, T. L., & Arimoto, R. (1996). Characterization of the Bermuda tropospheric aerosol by combined individual-particle and bulk-aerosol analysis. *Atmospheric Environment*, *30*(2), 319–338. https://doi.org/10.1016/1352-2310(95)00170-4

Andrews, E., Sheridan, P. J., Fiebig, M., McComiskey, A., Ogren, J. A., Arnott, P., et al. (2006). Comparison of methods for deriving aerosol asymmetry parameter. *Journal of Geophysical Research*, *111*(D5). https://doi.org/10.1029/2004jd005734

Arimoto, R. (2001). Eolian dust and climate: Relationships to sources, tropospheric chemistry, transport and deposition. *Earth-Science Reviews*, *54*(1), 29–42. https://doi.org/10.1016/s0012-8252(01)00040-x

Arimoto, R., Duce, R. A., Ray, B. J., & Tomza, U. (2003). Dry deposition of trace elements to the Western North Atlantic. *Global Biogeochemical Cycles*, *17*(1). https://doi.org/10.1029/2001gb001406

Aryal, R. P., Voss, K. J., Terman, P. A., Keene, W. C., Moody, J. L., Welton, E. J., & Holben, B. N. (2014). Comparison of surface and column measurements of aerosol scattering properties over the Western North Atlantic Ocean at Bermuda. *Atmospheric Chemistry and Physics*, *14*(14), 7617–7629. https://doi.org/10.5194/acp-14-7617-2014

Bennartz, R., & Rausch, J. (2017). Global and regional estimates of warm cloud droplet number concentration based on 13 years of Aqua-MODIS observations. *Atmospheric Chemistry and Physics*, *17*(16), 9815–9836. https://doi.org/10.5194/acp-17-9815-2017

Bi, J., Huang, J., Hu, Z., Holben, B. N., & Guo, Z. (2014). Investigating the aerosol optical and radiative characteristics of heavy Haze episodes in Beijing during January of 2013. *Journal of Geophysical Research - D: Atmospheres*, *119*(16), 9884–9900. https://doi.org/10.1002/2014jd021757

Bibi, H., Alam, K., Blaschke, T., Bibi, S., & Iqbal, M. J. (2016). Long-term (2007–2013) analysis of aerosol optical properties over four locations in the Indo-Gangetic plains. *Applied Optics*, *55*(23), 6199–6211. https://doi.org/10.1364/Ao.55.006199

Blyth, A. M., Lasher-Trapp, S. G., Cooper, W. A., Knight, C. A., & Latham, J. (2003). The role of giant and ultragiant nuclei in the formation of early radar echoes in warm Cumulus clouds. *Journal of the Atmospheric Sciences*, *60*(21), 2557–2572. https://doi.org/10.1175/1520-0469(2003)060<2557:trogau>2.0.co;2

Bosilovich, M., Lucchesi, R., & Suarez, M. (2015). *Merra-2*. File Specification.

Boucher, O. (1998). On aerosol direct shortwave forcing and the Henyey-Greenstein phase function. *Journal of the Atmospheric Sciences*, *55*(1), 128–134. https://doi.org/10.1175/1520-0469(1998)055<0128:Oadsfa>2.0.Co;2

Braun, R. A., Aghdam, M. A., Bañaga, P. A., Betito, G., Cambaliza, M. O., Cruz, M. T., et al. (2020). Long-range aerosol transport and impacts on size-resolved aerosol composition in Metro Manila, Philippines. *Atmospheric Chemistry and Physics*, *20*(4), 2387–2405. https://doi.org/10.5194/acp-20-2387-2020

Buchard, V., Randles, C. A., da Silva, A. M., Darmenov, A., Colarco, P. R., Govindaraju, R., et al. (2017). The Merra-2 aerosol reanalysis, 1980 onward. Part II: Evaluation and case studies. *Journal of Climate*, *30*(17), 6851–6872. https://doi.org/10.1175/Jcli-D-16-0613.1

Carlson, T. N., & Prospero, J. M. (1972). The large-scale movement of saharan air outbreaks over the Northern Equatorial Atlantic. *Journal of Applied Meteorology*, *11*(2), 283–297. https://doi.org/10.1175/1520-0450(1972)011<0283:TLSMOS>2.0.CO;2

Carslaw, K. S., Boucher, O., Spracklen, D. V., Mann, G. W., Rae, J. G. L., Woodward, S., & Kulmala, M. (2010). A review of natural aerosol interactions and feedbacks within the earth system. *Atmospheric Chemistry and Physics*, *10*(4), 1701–1737. https://doi.org/10.5194/acp-10-1701-2010

Carslaw, K. S., Gordon, H., Hamilton, D. S., Johnson, J. S., Regayre, L. A., Yoshioka, M., & Pringle, K. J. (2017). Aerosols in the pre-industrial atmosphere. *Current Climate Change Reports*, *3*(1), 1–15. https://doi.org/10.1007/s40641-017-0061-2

Che, H., Xia, X., Zhu, J., Wang, H., Wang, Y., Sun, J., et al. (2015). Aerosol optical properties under the condition of heavy Haze over an Urban Site of Beijing, China. *Environmental Science & Pollution Research*, *22*(2), 1043–1053. https://doi.org/10.1007/s11356-014-3415-5

Chubb, T., Huang, Y., Jensen, J., Campos, T., Siems, S., & Manton, M. (2016). Observations of high droplet number concentrations in southern ocean boundary layer clouds. *Atmospheric Chemistry and Physics*, *16*(2), 971–987. https://doi.org/10.5194/acp-16-971-2016

Corral, A. F., Braun, R. A., Cairns, B., Gorooh, V. A., Liu, H., Ma, L., et al. (2021). An overview of atmospheric features over the Western North Atlantic Ocean and North American East Coast—Part 1: Analysis of aerosols, gases, and wet deposition chemistry. *Journal of Geophysical Research: Atmospheres*, *126*. https://doi.org/10.1029/2020JD032592

Crosbie, E., Sorooshian, A., Monfared, N., Shingler, T., & Esmaili, O. (2014). A multi-year aerosol characterization for the greater Tehran area using satellite, surface, and modeling data. *Atmosphere*, *5*(2), 178–197. https://doi.org/10.3390/atmos5020178

Dadashazar, H., Ma, L., & Sorooshian, A. (2019). Sources of pollution and interrelationships between aerosol and precipitation chemistry at a Central California Site. *Science of the Total Environment*, *651*, 1776–1787. https://doi.org/10.1016/j.scitotenv.2018.10.086

Dadashazar, H., Wang, Z., Crosbie, E., Brunke, M., Zeng, X., Jonsson, H., et al. (2017). Relationships between Giant sea salt particles and clouds inferred from aircraft physicochemical data. *Journal of Geophysical Research - Atmospheres*, *122*(6), 3421–3434. https://doi.org/10.1002/2016jd026019

Delene, D. J., & Ogren, J. A. (2002). Variability of aerosol optical properties at four North American surface monitoring sites. *Journal of the Atmospheric Sciences*, *59*(6), 1135–1150. https://doi.org/10.1175/1520-0469(2002)059<1135:VOAOPA>2.0.CO;2

Dey, S., Tripathi, S. N., Singh, R. P., & Holben, B. N. (2004). Influence of dust storms on the aerosol optical properties over the Indo-Gangetic Basin. *Journal of Geophysical Research*, *109*(D20). https://doi.org/10.1029/2004jd004924

Dubovik, O., Holben, B., Eck, T. F., Smirnov, A., Kaufman, Y. J., King, M. D., et al. (2002). Variability of absorption and optical properties of key aerosol types observed in worldwide locations. *Journal of the Atmospheric Sciences*, *59*(3), 590–608. https://doi.org/10.1175/1520-0469(2002)059<0590:VOAAOP>2.0.CO;2

Dubovik, O., Smirnov, A., Holben, B. N., King, M. D., Kaufman, Y. J., Eck, T. F., & Slutsker, I. (2000). Accuracy assessments of aerosol optical properties retrieved from Aerosol Robotic Network (AERONET) Sun and Sky radiance measurements. *Journal of Geophysical Research*, *105*(D8), 9791–9806. https://doi.org/10.1029/2000JD900040

Eck, T. F., Holben, B. N., Dubovik, O., Smirnov, A., Goloub, P., Chen, H. B., et al. (2005). Columnar aerosol optical properties at AERONET sites in central eastern Asia and aerosol transport to the tropical mid-Pacific. *Journal of Geophysical Research*, *110*(D6). https://doi.org/10.1029/2004jd005274

Eck, T. F., Holben, B. N., Reid, J. S., Dubovik, O., Smirnov, A., O'Neill, N. T., et al. (1999). Wavelength dependence of the optical depth of biomass burning, urban, and desert dust aerosols. *Journal of Geophysical Research*, *104*(D24), 31333–31349. https://doi.org/10.1029/1999jd900923

Eck, T. F., Holben, B. N., Reid, J. S., Giles, D. M., Rivas, M. A., Singh, R. P., et al. (2012). Fog- and cloud-induced aerosol modification observed by the Aerosol Robotic Network (AERONET). *Journal of Geophysical Research*, *117*(D7). https://doi.org/10.1029/2011jd016839

Eck, T. F., Holben, B. N., Reid, J. S., O'Neill, N. T., Schafer, J. S., Dubovik, O., et al. (2003). High aerosol optical depth biomass burning events: A comparison of optical properties for different source regions. *Geophysical Research Letters*, *30*(20). https://doi.org/10.1029/2003gl017861

Eck, T. F., Holben, B. N., Sinyuk, A., Pinker, R. T., Goloub, P., Chen, H., et al. (2010). Climatological aspects of the optical properties of fine/coarse mode aerosol mixtures. *Journal of Geophysical Research*, *115*(D19). https://doi.org/10.1029/2010jd014002

Feingold, G., Cotton, W. R., Kreidenweis, S. M., & Davis, J. T. (1999). The impact of giant cloud condensation nuclei on drizzle formation in stratocumulus: Implications for cloud radiative properties. *Journal of the Atmospheric Sciences*, *56*(24), 4100–4117. https://doi.org/10.1175/1520-0469(1999)056<4100:tiogcc>2.0.co;2

Formenti, P., Andreae, M. O., & Lelieveld, J. (2000). Measurements of aerosol optical depth above 3570 M Asl in the North Atlantic free troposphere: Results from Ace-2. *Tellus B: Chemical and Physical Meteorology*, *52*(2), 678–693. https://doi.org/10.1034/j.1600-0889.2000.00006.x

Galloway, J. N., Artz, R. S., Dayan, U., Pueschel, R. F., & Boatman, J. F. (1988). WATOX-85: An aircraft and ground sampling program to determine the transport of trace gases and aerosols across the Western Atlantic Ocean. *Atmospheric Environment*, *22*(11), 2345–2360. https://doi.org/10.1016/0004-6981(88)90467-2

Galloway, J. N., Keene, W. C., Artz, R. S., Miller, J. M., Church, T. M., & Knap, A. H. (1989). Processes controlling the concentrations of SO=4, NO-3, NH+4, H+, HCOOT and CH3COOT in precipitation on Bermuda. *Tellus B: Chemical and Physical Meteorology*, *41*(4), 427–443. https://doi.org/10.3402/tellusb.v41i4.15098

Galloway, J. N., Knap, A. H., & Church, T. M. (1983). The composition of Western Atlantic precipitation using shipboard collectors. *Journal of Geophysical Research-Oceans*, *88*(Nc15), 859–864. https://doi.org/10.1029/jc088ic15p10859

Galloway, J. N., Savoie, D. L., Keene, W. C., & Prospero, J. M. (1993). The temporal and spatial variability of scavenging ratios for NSS sulfate, nitrate, methanesulfonate and sodium in the atmosphere over the North Atlantic Ocean. *Atmospheric Environment A. General Topics*, *27*(2), 235–250. https://doi.org/10.1016/0960-1686(93)90354-2

Gelaro, R., McCarty, W., Suárez, M. J., Todling, R., Molod, A., Takacs, L., et al. (2017). The modern-era retrospective analysis for research and applications, Version 2 (Merra-2). *Journal of Climate*, *30*(14), 5419–5454. https://doi.org/10.1175/JCLI-D-16-0758.1

Giles, D. M., Sinyuk, A., Sorokin, M. G., Schafer, J. S., Smirnov, A., Slutsker, I., et al. (2019). Advancements in the Aerosol Robotic Network (AERONET) Version 3 database - automated near-real-time quality control algorithm with improved cloud screening for Sun photometer aerosol optical depth (AOD) measurements. *Atmospheric Measurement Techniques*, *12*(1), 169–209. https://doi.org/10.5194/amt-12-169-2019

Gkikas, A., Hatzianastassiou, N., & Mihalopoulos, N. (2009). Aerosol events in the broader Mediterranean basin based on 7-year (2000-2007) MODIS C005 data. *AnnAls of Geophysics*, *27*(9), 3509–3522. https://doi.org/10.5194/angeo-27-3509-2009

Government of Bermuda (2019). *2016 population and Housing Census report*. Retrieved from https://www.gov.bm/articles/2016-population-and-housing-census-report

Grosvenor, D. P., Sourdeval, O., Zuidema, P., Ackerman, A., Alexandrov, M. D., Bennartz, R., et al. (2018). Remote sensing of droplet number concentration in warm clouds: A review of the current state of knowledge and perspectives. *RevIews of Geophysics*, *56*(2), 409–453. https://doi.org/10.1029/2017rg000593

Guishard, M. P., Nelson, E. A., Evans, J. L., Hart, R. E., & O'Connell, D. G. (2007). Bermuda subtropical storms. *Meteorology and Atmospheric Physics*, *97*(1), 239–253. https://doi.org/10.1007/s00703-006-0255-y

Hartley, W. S., & Hobbs, P. V. (2001). An aerosol model and aerosol-induced changes in the clear-sky albedo off the east coast of the United States. *Journal of Geophysical Research*, *106*(D9), 9733–9748. https://doi.org/10.1029/2001jd900025

Herber, A., Thomason, L. W., Gernandt, H., Leiterer, U., Nagel, D., Schulz, K.-H., et al. (2002). Continuous day and night aerosol optical depth observations in the Arctic between 1991 and 1999. *Journal of Geophysical Research*, *107*(D10), 6. https://doi.org/10.1029/2001jd000536

Hersey, S. P., Garland, R. M., Crosbie, E., Shingler, T., Sorooshian, A., Piketh, S., & Burger, R. (2015). An overview of regional and local characteristics of aerosols in South Africa using satellite, ground, and modeling data. *Atmospheric Chemistry and Physics*, *15*(8), 4259–4278. https://doi.org/10.5194/acp-15-4259-2015

Hilario, M. R. A., Cruz, M. T., Bañaga, P. A., Betito, G., Braun, R. A., Stahl, C., et al. (2020). Characterizing weekly cycles of particulate matter in a coastal megacity: The importance of a seasonal, size-resolved, and chemically speciated analysis. *Journal of Geophysical Research-Atmospheres*, *125*(13). https://doi.org/10.1029/2020JD032614

Hogan, T., Liu, M., Ridout, J., Peng, M., Whitcomb, T., Ruston, B., et al. (2014). The navy global environmental model. *Oceanography*, *27*(3), 116–125. https://doi.org/10.5670/oceanog.2014.73

Holben, B. N., Eck, T. F., Slutsker, I., Tanré, D., Buis, J. P., Setzer, A., et al. (1998). AERONET—A federated instrument network and data archive for aerosol characterization. *Remote Sensing of Environment*, *66*(1), 1–16. https://doi.org/10.1016/s0034-4257(98)00031-5

Holben, B. N., Tanré, D., Smirnov, A., Eck, T. F., Slutsker, I., Abuhassan, N., et al. (2001). An emerging ground-based aerosol climatology: Aerosol optical depth from AERONET. *Journal of Geophysical Research*, *106*(D11), 12067–12097. https://doi.org/10.1029/2001jd900014

Hoppel, W. A., Fitzgerald, J. W., Frick, G. M., Larson, R. E., & Mack, E. J. (1990). Aerosol size distributions and optical properties found in the marine boundary layer over the Atlantic Ocean. *Journal of Geophysical Research*, *95*(D4), 3659–3686. https://doi.org/10.1029/JD095iD04p03659

Horvath, H., Gunter, R. L., & Wilkison, S. W. (1990). Determination of the coarse mode of the atmospheric aerosol using data from a forward-scattering spectrometer probe. *Aerosol Science and Technology*, *12*(4), 964–980. https://doi.org/10.1080/02786829008959407

Hsu, K.-l., Gao, X., Sorooshian, S., & Gupta, H. V. (1997). Precipitation estimation from remotely sensed information using artificial neural networks. *Journal of Applied Meteorology 36*(9), 1176–1190. https://doi.org/10.1175/1520-0450(1997)036<1176:PEFRSI>2.0.CO;2

Iftikhar, M., Alam, K., Sorooshian, A., Syed, W. A., Bibi, S., & Bibi, H. (2018). Contrasting aerosol optical and radiative properties between dust and urban Haze episodes in megacities of Pakistan. *Atmospheric Environment*, *173*, 157–172. https://doi.org/10.1016/j.atmosenv.2017.11.011

IPCC. (2013). *Climate change 2013: The Physical Science basis*. Cambridge.

Jickells, T., Knap, A., Church, T., Galloway, J., & Miller, J. (1982). Acid rain on Bermuda. *Nature*, *297*(5861), 55–57. https://doi.org/10.1038/297055a0

Jose, S., Gharai, B., Niranjan, K., & Rao, P. V. N. (2016). Investigation on seasonal variations of aerosol properties and its influence on radiative effect over an urban location in Central India. *Atmospheric Environment*, *133*, 41–48. https://doi.org/10.1016/j.atmosenv.2016.03.029

Jung, E., Albrecht, B. A., Jonsson, H. H., Chen, Y.-C., Seinfeld, J. H., Sorooshian, A., et al. (2015). Precipitation effects of giant cloud condensation nuclei artificially introduced into stratocumulus clouds. *Atmospheric Chemistry and Physics*, *15*(10), 5645–5658. https://doi.org/10.5194/acp-15-5645-2015

Kaskaoutis, D. G., Kosmopoulos, P., Kambezidis, H. D., & Nastos, P. T. (2007). Aerosol climatology and discrimination of different types over Athens, Greece, based on MODIS data. *Atmospheric Environment*, *41*(34), 7315–7329. https://doi.org/10.1016/j.atmosenv.2007.05.017

Keene, W. C., Maring, H., Maben, J. R., Kieber, D. J., Pszenny, A. A. P., Dahl, E. E., et al. (2007). Chemical and physical characteristics of nascent aerosols produced by bursting bubbles at a model air–sea interface. *Journal of Geophysical Research*, *112*(D21). https://doi.org/10.1029/2007jd008464

Keene, W. C., Moody, J. L., Galloway, J. N., Prospero, J. M., Cooper, O. R., Eckhardt, S., & Maben, J. R. (2014). Long-term trends in aerosol and precipitation composition over the Western North Atlantic Ocean at Bermuda. *Atmospheric Chemistry and Physics*, *14*(15), 8119–8135. https://doi.org/10.5194/acp-14-8119-2014

Kim, Y., Sievering, H., & Boatman, J. (1990). Volume and surface area size distribution, water mass and model fitting of GCE/CASE/WATOX marine aerosols. *Global Biogeochemical Cycles*, *4*(2), 165–177. https://doi.org/10.1029/gb004i002p00165

Kinne, S. (2019). The Macv2 aerosol climatology. *Tellus B: Chemical and Physical Meteorology*, *71*, 1–21. https://doi.org/10.1080/16000889.2019.1623639

Korotaev, G. K., Sakerin, S. M., Ignatov, A. M., Stowe, L. L., & McClain, E. P. (1993). Sun-photometer observations of aerosol optical thickness over the North Atlantic from a Soviet research vessel for validation of satellite measurements. *Journal of Atmospheric and Oceanic Technology.*, *10*(5), 725–735. https://doi.org/10.1175/1520-0426(1993)010<0725:SPOOAO>2.0.CO;2

Kramer, S. J., Alvarez, C., Barkley, A. E., Colarco, P. R., Custals, L., Delgadillo, R., et al. (2020). Apparent dust size discrepancy in aerosol reanalysis in North African dust after long-range transport. *Atmospheric Chemistry and Physics*, *20*(16), 10047–10062. https://doi.org/10.5194/acp-20-10047-2020

Kumar, K. R., Sivakumar, V., Reddy, R. R., Gopal, K. R., & Adesina, A. J. (2014). Identification and classification of different aerosol types over a subtropical rural site in Mpumalanga, South Africa: Seasonal variations as retrieved from the AERONET Sunphotometer. *Aerosol and Air Quality Research*, *14*(1), 108–123. https://doi.org/10.4209/aaqr.2013.03.0079

Kumar, K. R., Yin, Y., Sivakumar, V., Kang, N., Yu, X., Diao, Y., et al. (2015). Aerosol climatology and discrimination of aerosol types retrieved from MODIS, MISR and OMI over Durban (29.88°S, 31.02°E), South Africa. *Atmospheric Environment*, *117*, 9–18. https://doi.org/10.1016/j.atmosenv.2015.06.058

Lopez, D., Rabbani, M., Crosbie, E., Raman, A., Arellano, A., & Sorooshian, A. (2016). Frequency and character of extreme aerosol events in the Southwestern United States: A case study analysis in Arizona. *Atmosphere*, *7*(1), 1. https://doi.org/10.3390/atmos7010001

Lynch, P., Reid, J. S., Westphal, D. L., Zhang, J., Hogan, T. F., Hyer, E. J., et al. (2016). An 11-year global gridded aerosol optical thickness reanalysis (V1.0) for atmospheric and climate sciences. *Geoscientific Model Development*, *9*(4), 1489–1522. https://doi.org/10.5194/gmd-9-1489-2016

Ma, L., Dadashazar, H., Hilario, M. R. A., Cambaliza, M. O., Lorenzo, G. R., Simpas, J. B., et al. (2021). Contrasting wet deposition composition between three diverse islands and coastal North American sites. *Atmospheric Environment*, *244*, 117919. https://doi.org/10.1016/j.atmosenv.2020.117919

Mardi, A. H., Dadashazar, H., MacDonald, A. B., Braun, R. A., Crosbie, E., Xian, P., et al. (2018). Biomass burning plumes in the vicinity of the california coast: Airborne characterization of physicochemical properties, heating rates, and spatiotemporal features. *Journal of Geophysical Research - D: Atmospheres*, *123*(23), 13560–13582. https://doi.org/10.1029/2018jd029134

Maudlin, L. C., Wang, Z., Jonsson, H. H., & Sorooshian, A. (2015). Impact of wildfires on size-resolved aerosol composition at a coastal California site. *Atmospheric Environment*, *119*, 59–68. https://doi.org/10.1016/j.atmosenv.2015.08.039

Mead, C., Herckes, P., Majestic, B. J., & Anbar, A. D. (2013). Source apportionment of aerosol iron in the marine environment using iron isotope analysis. *Geophysical Research Letters*, *40*(21), 5722–5727. https://doi.org/10.1002/2013gl057713

Merrill, J. T. (1994). Isentropic airflow probability analysis. *Journal of Geophysical Research*, *99*(D12), 25881–25889. https://doi.org/10.1029/94jd02211

Miller, J. M., & Harris, J. M. (1985). The flow climatology to Bermuda and its implications for long-range transport. *Atmospheric Environment*, *19*(3), 409–414. https://doi.org/10.1016/0004-6981(85)90162-3

Minnis, P., Sun-Mack, S., Chen, Y., Chang, F.-L., Yost, C. R., Smith, W. L., et al. (2021). CERES MODIS Cloud product retrievals for Edition 4—Part I: Algorithm changes. *IEEE Transactions on Geoscience and Remote Sensing*, *59*, 2744–2780. https://doi.org/10.1109/TGRS.2020.3008866

Minnis, P., Sun-Mack, S., Young, D. F., Heck, P. W., Garber, D. P., Chen, Y., et al. (2011). Ceres edition-2 cloud property retrievals using TRMM VIRS and Terra and Aqua MODIS Data—Part I: Algorithms. *IEEE Transactions on Geoscience and Remote Sensing*, *49*(11), 4374–4400. https://doi.org/10.1109/Tgrs.2011.2144601

Moody, J. L., & Galloway, J. N. (1988). Quantifying the relationship between atmospheric transport and the chemical composition of precipitation on Bermuda. *Tellus B: Chemical and Physical Meteorology*, *40*(5), 463–479. https://doi.org/10.3402/tellusb.v40i5.16014

Moody, J. L., Oltmans, S. J., Levy, H., II, & Merrill, J. T. (1995). Transport climatology of tropospheric ozone: Bermuda, 1988–1991. *Journal of Geophysical Research*, *100*, 7179–7194. https://doi.org/10.1029/94jd02830

Mora, M., Braun, R. A., Shingler, T., & Sorooshian, A. (2017). Analysis of remotely sensed and surface data of aerosols and meteorology for the Mexico Megalopolis area between 2003 and 2015. *Journal of Geophysical Research - Atmospheres*, *122*(16), 8705–8723. https://doi.org/10.1002/2017jd026739

Muhs, D. R., Budahn, J. R., Prospero, J. M., Skipp, G., & Herwitz, S. R. (2012). Soil genesis on the island of Bermuda in the quaternary: The importance of African dust transport and deposition. *Journal of Geophysical Research-Earth Surface*, *117*. https://doi.org/10.1029/2012jf002366

Nguyen, P., Shearer, E. J., Tran, H., Ombadi, M., Hayatbini, N., Palacios, T., et al. (2019). The CHRS data portal, an easily accessible public repository for PERSIANN global satellite precipitation data. *Scientific Data*, *6*(1), 180296. https://doi.org/10.1038/sdata.2018.296

Pace, G., di Sarra, A., Meloni, D., Piacentino, S., & Chamard, P. (2006). Aerosol optical properties at Lampedusa (Central Mediterranean). 1. Influence of transport and identification of different aerosol types. *Atmospheric Chemistry and Physics*, *6*(3), 697–713. https://doi.org/10.5194/acp-6-697-2006

Painemal, D. (2018). Global estimates of changes in shortwave low-cloud albedo and fluxes due to variations in cloud droplet number concentration derived from CERES-MODIS satellite sensors. *Geophysical Research Letters*, *45*(17), 9288–9296. https://doi.org/10.1029/2018gl078880

Painemal, D., Corral, A. F., Sorooshian, A., Brunke, M. A., Chellappan, S., Afzali Gorooh, V., et al. (2021). An overview of atmospheric features over the Western North Atlantic Ocean and North American East Coast—Part 2: Circulation, boundary layer, and clouds. *Journal of Geophysical Research: Atmospheres*, *126*. https://doi.org/10.1029/2020JD033423

Painemal, D., Minnis, P., & Sun-Mack, S. (2013). The impact of horizontal heterogeneities, cloud fraction, and liquid water path on warm cloud effective radii from Ceres-Like Aqua Modis retrievals. *Atmospheric Chemistry and Physics*, *13*(19), 9997–10003. https://doi.org/10.5194/acp-13-9997-2013

Pandolfi, M., Alados-Arboledas, L., Alastuey, A., Andrade, M., Angelov, C., Artiñano, B., et al. (2018). A european aerosol phenomenology—6: Scattering properties of atmospheric aerosol particles from 28 ACTRIS sites. *Atmospheric Chemistry and Physics*, *18*(11), 7877–7911. https://doi.org/10.5194/acp-18-7877-2018

Perry, K. D., Cahill, T. A., Eldred, R. A., Dutcher, D. D., & Gill, T. E. (1997). Long-range transport of North African dust to the Eastern United States. *Journal of Geophysical Research*, *102*(D10), 11225–11238. https://doi.org/10.1029/97jd00260

Prasad, A. K., & Singh, R. P. (2007). Changes in aerosol parameters during major dust storm events (2001–2005) over the Indo-Gangetic Plains using AERONET and MODIS data. *Journal of Geophysical Research*, *112*(D9). https://doi.org/10.1029/2006jd007778

Prospero, J. M. (1999). Long-Term measurements of the transport of African mineral dust to the Southeastern United States: Implications for regional air quality. *Journal of Geophysical Research*, *104*(D13), 15917–15927. https://doi.org/10.1029/1999jd900072

Prospero, J. M., & Landing, W. (2009). African dust deposition to Florida: How well do dust models perform? *IOP Conference Series: Earth and Environmental Science*, *7*, 012015. https://doi.org/10.1088/1755-1307/7/1/012015

Randles, C. A., da Silva, A. M., Buchard, V., Colarco, P. R., Darmenov, A., Govindaraju, R., et al. (2017). The Merra-2 Aerosol reanalysis, 1980 onward. Part I: System description and data assimilation evaluation. *Journal of Climate*, *30*(17), 6823–6850. https://doi.org/10.1175/Jcli-D-16-0609.1

Reddy, P. J., Kreiner, F. W., DeLuisi, J. J., & Kim, Y. (1990). Aerosol optical depths over the atlantic derived from Shipboard Sunphotometer observations during the 1988 global change expedition. *Global Biogeochemical Cycles*, *4*(3), 225–240. https://doi.org/10.1029/gb004i003p00225

Regayre, L. A., Schmale, J., Johnson, J. S., Tatzelt, C., Baccarini, A., Henning, S., et al. (2020). The value of remote marine aerosol measurements for constraining radiative forcing uncertainty. *Atmospheric Chemistry and Physics*, *20*(16), 10063–10072. https://doi.org/10.5194/acp-20-10063-2020

Reid, J. S., Koppmann, R., Eck, T. F., & Eleuterio, D. P. (2005). A review of biomass burning emissions. Part II: Intensive physical properties of biomass burning particles. *Atmospheric Chemistry and Physics*, *5*, 799–825. https://doi.org/10.5194/acp-5-799-2005

Rienecker, M. M., Suarez, M. J., Gelaro, R., Todling, R., Bacmeister, J., Liu, E., et al. (2011). Merra: Nasa's modern-era retrospective analysis for research and applications. *Journal of Climate*, *24*(14), 3624–3648. https://doi.org/10.1175/Jcli-D-11-00015.1

Rolph, G., Stein, A., & Stunder, B. (2017). Real-time environmental applications and display system: Ready. *Environmental Modelling & Software*, *95*, 210–228. https://doi.org/10.1016/j.envsoft.2017.06.025

Ross, J. L., Hobbs, P. V., & Holben, B. (1998). Radiative characteristics of regional Hazes dominated by smoke from biomass burning in Brazil: Closure tests and direct radiative forcing. *Journal of Geophysical Research*, *103*(D24), 31925–31941. https://doi.org/10.1029/97jd03677

Russell, P. B., Kinne, S. A., & Bergstrom, R. W. (1997). Aerosol climate effects: Local radiative forcing and column closure experiments. *Journal of Geophysical Research*, *102*(D8), 9397–9407. https://doi.org/10.1029/97jd00112

Salinas, S. V., Chew, B. N., Miettinen, J., Campbell, J. R., Welton, E. J., Reid, J. S., et al. (2013). Physical and optical characteristics of the October 2010 Haze Event over Singapore: A photometric and lidar analysis. *Atmospheric Research*, *122*, 555–570. https://doi.org/10.1016/j.atmosres.2012.05.021

Schlosser, J. S., Braun, R. A., Bradley, T., Dadashazar, H., MacDonald, A. B., Aldhaif, A. A., et al. (2017). Analysis of Aerosol composition data for Western United States Wildfires between 2005 and 2015: Dust emissions, chloride depletion, and most enhanced aerosol constituents. *Journal of Geophysical Research - D: Atmospheres*, *122*(16), 8951–8966. https://doi.org/10.1002/2017jd026547

Schuster, G. L., Dubovik, O., & Holben, B. N. (2006). Angstrom exponent and bimodal aerosol size distributions. *Journal of Geophysical Research*, *111*(D7). https://doi.org/10.1029/2005jd006328

Sharma, M., Kaskaoutis, D. G., Singh, R. P., & Singh, S. (2014). Seasonal variability of atmospheric aerosol parameters over greater noida using ground sunphotometer observations. *Aerosol and Air Quality Research*, *14*(3), 608–622. https://doi.org/10.4209/aaqr.2013.06.0219

Smirnov, A., Holben, B. N., Dubovik, O., Frouin, R., Eck, T. F., & Slutsker, I. (2003). Maritime component in aerosol optical models derived from aerosol robotic network data. *Journal of Geophysical Research*, *108*(D1). https://doi.org/10.1029/2002jd002701

Smirnov, A., Holben, B. N., Dubovik, O., O'Neill, N. T., Remer, L. A., Eck, T. F., et al. (2000). Measurement of atmospheric optical parameters on U.S. Atlantic coast sites, ships, and Bermuda during TARFOX. *Journal of Geophysical Research*, *105*(D8), 9887–9901. https://doi.org/10.1029/1999jd901067

Smirnov, A., Holben, B. N., Kaufman, Y. J., Dubovik, O., Eck, T. F., Slutsker, I., et al. (2002). Optical properties of atmospheric aerosol in maritime environments. *Journal of the Atmospheric Sciences*, *59*(3), 501–523. https://doi.org/10.1175/1520-0469(2002)059<0501:OPOAAI>2.0.CO;2

Smirnov, A., Holben, B. N., Slutsker, I., Welton, E. J., & Formenti, P. (1998). Optical properties of Saharan dust during Ace 2. *Journal of Geophysical Research*, *103*(D21), 28079–28092. https://doi.org/10.1029/98jd01930

Smirnov, A., Villevalde, Y., O'Neill, N. T., Royer, A., & Tarussov, A. (1995). Aerosol optical depth over the oceans: Analysis in terms of synoptic air mass types. *Journal of Geophysical Research*, *100*(D8), 16639–16650. https://doi.org/10.1029/95jd01265

Sorooshian, A., Anderson, B., Bauer, S. E., Braun, R. A., Cairns, B., Crosbie, E., et al. (2019). Aerosol-cloud-meteorology interaction airborne field investigations: Using lessons learned from the U.S. West Coast in the design of ACTIVATE off the U.S. East Coast. *Bulletin of the American Meteorological Society*, *100*(8), 1511–1528. https://doi.org/10.1175/Bams-D-18-0100.1

Sorooshian, A., Corral, A. F., Braun, R. A., Cairns, B., Crosbie, E., Ferrare, R., et al. (2020). Atmospheric research over the Western North Atlantic ocean region and North American East Coast: A review of past work and challenges ahead. *Journal of Geophysical Research - D: Atmospheres*, *125*(6). https://doi.org/10.1029/2019JD031626

Sorooshian, A., Crosbie, E., Maudlin, L. C., Youn, J. S., Wang, Z., Shingler, T., et al. (2015). Surface and airborne measurements of organosulfur and methanesulfonate over the Western United States and Coastal Areas. *Journal of Geophysical Research - D: Atmospheres*, *120*(16), 8535–8548. https://doi.org/10.1002/2015jd023822

Sorooshian, A., Wang, Z., Feingold, G., & L'Ecuyer, T. S. (2013). A satellite perspective on cloud water to rain water conversion rates and relationships with environmental conditions. *Journal of Geophysical Research - D: Atmospheres*, *118*(12), 6643–6650. https://doi.org/10.1002/jgrd.50523

Sorooshian, A., Wonaschütz, A., Jarjour, E. G., Hashimoto, B. I., Schichtel, B. A., & Betterton, E. A. (2011). An aerosol climatology for a rapidly growing arid region (Southern Arizona): Major aerosol species and remotely sensed aerosol properties. *Journal of Geophysical Research*, *116*. https://doi.org/10.1029/2011jd016197

Stein, A. F., Draxler, R. R., Rolph, G. D., Stunder, B. J. B., Cohen, M. D., & Ngan, F. (2015). Noaa's hysplit atmospheric transport and dispersion modeling system. *Bulletin of the American Meteorological Society*, *96*(12), 2059–2077. https://doi.org/10.1175/BAMS-D-14-00110.1

Tackett, J. L., Winker, D. M., Getzewich, B. J., Vaughan, M. A., Young, S. A., & Kar, J. (2018). CALIPSO Lidar Level 3 Aerosol profile product: Version 3 algorithm design. *Atmospheric Measurement Techniques*, *11*(7), 4129–4152. https://doi.org/10.5194/amt-11-4129-2018

Uchiyama, A., Yamazaki, A., Kudo, R., Kobayashi, E., Togawa, H., & Uesawa, D. (2014). Continuous ground-based observation of aerosol optical properties at Tsukuba, Japan: Trend and climatology. *Journal of the Meteorological Society of Japan*, *92a*, 93–108. https://doi.org/10.2151/jmsj.2014-A06

Vaughan, M. A., Powell, K. A., Winker, D. M., Hostetler, C. A., Kuehn, R. E., Hunt, W. H., et al. (2009). Fully automated detection of cloud and aerosol layers in the CALIPSO Lidar measurements. *Journal of Atmospheric and Oceanic Technology*, *26*(10), 2034–2050. https://doi.org/10.1175/2009jtecha1228.1

Villevalde, Y. V., Smirnov, A. V., O'Neill, N. T., Smyshlyaev, S. P., & Yakovlev, V. V. (1994). Measurement of aerosol optical depth in the Pacific Ocean and the North Atlantic. *Journal of Geophysical Research*, *99*(D10), 20983–20988. https://doi.org/10.1029/94jd01618

Wadleigh, M. A. (2004). Sulfur isotopic composition of aerosols over the Western North Atlantic Ocean. *Canadian Journal of Fisheries and Aquatic Sciences*, *61*(5), 817–825. https://doi.org/10.1139/f04-073

Wang, Y. Q., Zhang, X. Y., & Draxler, R. R. (2009). TrajStat: Gis-based software that uses various trajectory statistical analysis methods to identify potential sources from long-term air pollution measurement data. *Environmental Modelling & Software*, *24*(8), 938–939. https://doi.org/10.1016/j.envsoft.2009.01.004

Wells, K. C., Witek, M., Flatau, P., Kreidenweis, S. M., & Westphal, D. L. (2007). An analysis of seasonal surface dust aerosol concentrations in the western US (2001–2004): Observations and model predictions. *Atmospheric Environment*, *41*(31), 6585–6597. https://doi.org/10.1016/j.atmosenv.2007.04.034

Winker, D. M., Vaughan, M. A., Omar, A., Hu, Y., Powell, K. A., Liu, Z., et al. (2009). Overview of the CALIPSO mission and CALIOP data processing algorithms. *Journal of Atmospheric and Oceanic Technology*, *26*(11), 2310–2323. https://doi.org/10.1175/2009jtecha1281.1

Wolff, G. T., Ruthkosky, M. S., Stroup, D. P., Korsog, P. E., Ferman, M. A., Wendel, G. J., & Stedman, D. H. (1986). Measurements of Sox, Nox and aerosol species on Bermuda. *Atmospheric Environment*, *20*(6), 1229–1239. https://doi.org/10.1016/0004-6981(86)90158-7

Wood, R. (2012). Stratocumulus clouds. *Monthly Weather Review*, *140*(8), 2373–2423. https://doi.org/10.1175/MWR-D-11-00121.1

Xian, P., Reid, J. S., Atwood, S. A., Johnson, R. S., Hyer, E. J., Westphal, D. L., & Sessions, W. (2013). Smoke aerosol transport patterns over the Maritime continent. *Atmospheric Research*, *122*, 469–485. https://doi.org/10.1016/j.atmosres.2012.05.006

Yu, X., Kumar, K. R., Lü, R., & Ma, J. (2016). Changes in column aerosol optical properties during extreme Haze-Fog episodes in January 2013 over Urban Beijing. *Environmental Pollution*, *210*, 217–226. https://doi.org/10.1016/j.envpol.2015.12.021

Zhuravleva, T. B., Bedareva, T. V., & Sviridenkov, M. A. (2013). Retrieval of aerosol microstructure and radiative properties for moderate turbidity under conditions of Western Siberia. *AIP Conference Proceedings*, *1531*(1), 147–150. https://doi.org/10.1063/1.4804728

Zuidema, P., Alvarez, C., Kramer, S. J., Custals, L., Izaguirre, M., Sealy, P., et al. (2019). Is summer African dust arriving earlier to Barbados? The updated long-term in situ dust mass concentration time series from ragged point, Barbados, and Miami, Florida. *Bulletin of the American Meteorological Society*, *100*(10), 1981–1986. https://doi.org/10.1175/Bams-D-18-0083.1